Studies on Yaw-Control of Heavy-Duty Trucks using Unilateral Braking

Gäfvert, Magnus

2001

Document Version:
Publisher's PDF, also known as Version of record

ISSN 0280–5316
ISRN LUTFD2/TFRT--7598--SE

DICOSMOS INTERNAL REPORT

Revision 1.0

Studies on Yaw-Control of Heavy-Duty Trucks using Unilateral Braking

Magnus Gäfvert

Department of Automatic Control
Lund Institute of Technology, Sweden

December 2001

Contents

1. Introduction

This report is part of the DICOSMOS2 project, under the Swedish NUTEK (VINNOVA) Complex Techical Systems Program. DICOSMOS2 is a joint effort between the Department of Automatic Control (LTH), Mechatronics/Department of Machine Design (KTH), the Department of Computer Engineering (CTU), and Volvo Technological Development (VTD). The project is aimed at the study of distributed control of safety-critical motion systems. Part of the DICOSMOS2 is a study on the design of distributed real-time control systems on vehicles, initiated by VTD. An active yaw-control system for a tractor-semitrailer commercial vehicle was selected as a case study. This report is part of the results from the case study. More results are found in [SCG00, CGS00, GSC00, GL01].

The introduction of communication network infrastructures and computers in heavy commercial vehicles opens doors to new active safety systems based on the integration of previously autonomous systems. In passenger cars the introduction of such systems in production vehicles started several years ago with the introduction of integrated anti-lock braking systems (ABS), traction control systems (TCS), active yaw control systems (AYC, ESP) etc. The commercial vehicles industry has been slower to adopt this trend. Among the reasons for this is the stricter economical constraints the on commercial vehicle market, with respect to low vehicle price, low maintenance, and high dependability. The commercial vehicle market is also more conservative to new technology. An excellent overview of active safety systems in commercial vehicles and the specific conditions they are exposed to is found in[PF01].

This study is devoted to active yaw-control systems based on unilateral braking on tractor-semitrailer vehicle combinations. These systems have recently been introduced on production commercial vehicles. The switch to the faster and more easily controlled Electrical Braking Systems (EBS) [Ban99] has been a key factor in making this technology available on heavy vehicles. The majority of work published on AYC is applications on passenger cars. Many of the results are transferable to commercial vehicles, but there are also important differences such as the issues of roll-over due to high center of gravity, slower braking dynamics and combinations of tractors and trailers. Since published work on commercial vehicle AYC often focus on the differences from car AYC it is good to start with a survey on passenger car AYC systems. First the basic principles of AYC will be presented.

1.1 Principles

The motivation behind AYC systems is the observation that averagely skilled drivers rarely know when they are driving their cars near the physical limit for stability. This limit is due to the limited adhesion forces available between the tires and the road. While the tyre-road contact forces are reasonably linear within the adhesion limits, they become highly nonlinear at the limits, and the driver will not recognize the behaviour of his/her vehicle. The result is an unstable car that is understeering or oversteering, and a driver with lost control. The adhesion limits are strongly dependent on the road surface conditions.

The vehicle motion may be described by three states: the longitudinal velocity U and the lateral velocity V of the center of mass (CM),

and the yaw rate r, see Figure 1. For articulated vehicles such as the tractor-semitrailer vehicle combination the articulation angle ψ, and the articulation angular velocity $\dot{\psi}$ are additional state variables. The vehicle side-slip β, is defined as $\beta = V/U$ (small angles). The tyre-road contact force is a function of the tyre slip. The tyre slip has a lateral and a longitudinal component. Commonly, the lateral component is represented by the tyre slip-angle $\alpha = v/u$ (for small angles), where u and v are the longitudinal and lateral velocities of the wheel over ground, while the longitudinal component is represented by the normalized longitudinal tyre slip $\lambda = (R_w\omega - u)/u$, where R_w is the wheel radius, ω the wheel angular velocity. The lateral adhesion force Y at free-rolling cornering depends on the slip angle α. For small α the lateral force is approximately proportional to α as $Y = C_\alpha\alpha$, while at larger α the lateral force adhesion limit is reached, and the adhesion force saturates at a maximum $Y = Y^*$. Likewise, for small λ the longitudinal adhesion force X at straight driving is approximately proportional to λ as $X = C_\lambda\lambda$, while at larger λ the adhesion limit is reached, and the adhesion force saturates at a maximum $X = X^*$. At combined cornering and braking the available adhesion force is limited, approximately within the ellipse $(X/X^*)^2 + (Y/Y^*)^2 < 1$.

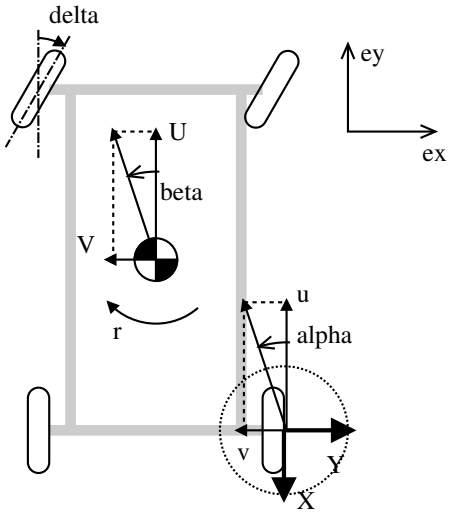

Figure 1 Illustration of velocities and forces on the car.

At normal driving the lateral adhesion forces are stabilizing the vehicle along the desired path determined by the drivers steering wheel input. At the adhesion limits these forces are saturated, and the vehicle becomes unstable. If the front axle wheels loose adhesion understeering will result, if the rear axle wheels loose adhesion tha car will oversteer and possibly spin out, see Figure 2.

The basic principle of AYC systems is to limit the side-slip angles α, such that the adhesion limits are not reached, and to replace the lost stabilizing lateral tire forces with stabilizing longitudinal tire forces. These forces are generated by unilateral braking actions. Instead of limiting the tire side-slips directly, the vehicle slip β is often the controlled variable. Limiting β is the same as keeping the vehicle oriented in the direction of velocity (the vector $[U, V]^T$). The controlled braking actions then result in

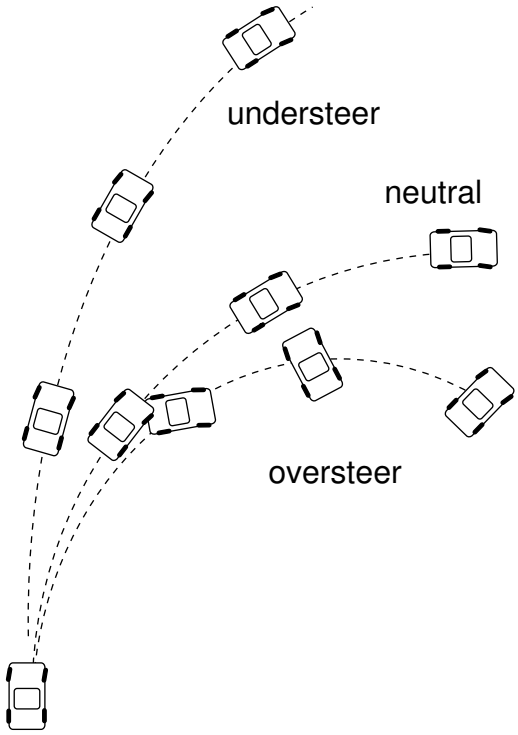

Figure 2 Illustration of car behaviours at tyre adhesion limits.

moments that strive to turn the car such that the side-slip is limited. To follow a curvature path it is also desireable to control the yaw rate r. Since also the longitudinal actuation forces X are subject to physical adhesion limits, it is not possible for the controlled vehicle to follow arbitrary paths. The AYC may improve the behaviour near the adhesion limits, but when the limits are severely violated stability of the vehicle will be lost.

1.2 Passenger Cars

The first publications on AYC appeared in the early 90's. In the early theoretical work [SST93] from Honda the authors introduce the β-method, by which the vehicle side-slip is used to explain the difficulties in maneuvering a car at the adhesion limits. Special attention is payed to acceleration and deceleration situations. A control law where unilateral braking actions are proportional to the lateral acceleration is demonstrated to improve vehicle stability. Application of these ideas are presented in a work from Mitsubishi [IS95], where a simple PI yaw-rate controller with unilateral brake actuation is shown to improve stability in accelerating and decelerating cornering. Bosch presented the Vehicle Dynamics Control (VDC) concept in [vZEP95]. This paper describes a complete hiearchical control system with yaw-moment control on top of local brake slip controllers. The yaw moment controller is an LQ state-feedback controller on the yaw-rate and side-slip states with a nominal moment as controller output. This moment is then mapped on local slip-controllers as slip-references. The local

brake slip controllers are robust PID controllers. Test results are presented that shows how the system improves stability in lane change and cornering maneuvers. An overview of the implementation of a production VDC system is also provided. Practical issues on the system hardware is elaborated in [vZELP98]. This article also includes a description of the VDC systems fault-tolerance properties. In [vZ00] experiences and updates of the Bosch EPS (or VDC) system is presented. An evaluation of AYC based on yaw-rate feedback or yaw-rate and side-slip feedback is presented in [Hac98]. The studied controllers are PD controllers with nominal moments as outputs. It is concluded that the combination of yaw-rate and side-slip control is superior on slippery surfaces. General Motors describes an implementation of a Delphi Automotive VDC system in [HR98]. Application of H_∞-control theory on AYC is presented in [PA99]. Robust stability by μ-analysis is performed. Results are demonstrated in simulations. Sliding mode theory is applied in [YAB+99]. The controllers are evaluated in field-tests. Another application of sliding mode theory is found in [DAR00]. This is a purely theoretical work without any validation of the proposed algorithm.

1.3 Commercial Vehicles

An early work is [PEG95], in which AYC is realized by LQR state-feedback controllers on the tractor semitrailer state $(\beta, r, \dot{\psi}, \psi)^T$, with a nominal moment as controller output. Sensitivity analysis on model parameters is provided, and is followed by a new robust RLQR controller design. The results are evaluated in simulations. Bosch entered the commercial vehicles VDC scene with [HHJ+97]. The presented systems shows large similarities with the Bosch VDC system for passenger cars. The additional states to control for articulated vehicles are mentioned, but it is not clear wether they are part of the control algorithm. WABCO presents a their concept of AYC on commercial vehicles in [PNG+98]. A hardware-in-the-loop simulation study of AYC on a tractor-semitrailer vehicle is presented. The actual controller used are not described, but yaw-rate and lateral acceleration sensors are included in the system. In [MSH+99] AYC of non-articulated heavy vehicles is studied by Mitsubishi engineers. Differences from passenger cars control are highlighted. The authors conclude that AYC is effective also on heavy vehicles.

2. Vehicle Models

This section presents a set of models suitable for the analysis of yaw control strategies. Models for non-articulated vehicles such as passenger cars and tractors are treated, as well as models for the articulated tractor-semitrailer vehicle combination. Linear chassis models are suitable for controller design, whereas nonlinear models should be used for validation. Good modelling of tire adhesion forces is necessary in the context of yaw control. Therefore several tire models will be presented and discussed.

2.1 Tractor Dynamics

Regard the vehicle of Figure 3 with mass m and moment of inertia J. This may represent a passenger car or an non-articulated truck. The planar

equations of motion for the vehicle can be stated as [GSC00]

$$m\left(\dot{U} - \dot{r}y - r^2x - rV\right) = X \tag{1a}$$
$$m\left(\dot{V} + \dot{r}x - r^2y + rU\right) = Y \tag{1b}$$
$$J\dot{r} + mx\left(\dot{V} + Ur\right) - my\left(\dot{U} - Vr\right) = M \tag{1c}$$

where V and r are the lateral velocity and yaw rate at origo O. The CM location is $[x, y]^T$. For a car it is convenient to locate the origo at the CM such that $x = 0$, $y = 0$. Assuming lateral symmetry in the mass distribution, and constant longitudinal speed, the equations are simplified to the linear dynamics

$$m\dot{V} = -mUr + Y \tag{2a}$$
$$J\dot{r} = M \tag{2b}$$

The longitudinal speed U will be regarded as constant. Let X_i and Y_i denote the longitudinal and lateral tire forces at wheel i. Let wheel i be located at coordinates (a_i, b_i) with respect to the CM. Then the external moments acting on the vehicle are $M = \sum_i -b_iX_i + a_iY_i$. Denote the lon-

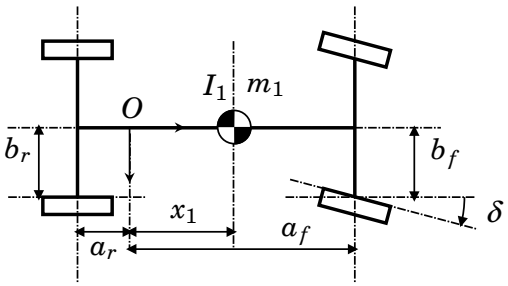

Figure 3 Geometry of the car.

gitudinal slip for wheel i with λ_i and the side-slip angle by α_i. The longitudinal slip is defined as

$$\lambda_i = \omega R_i/U - 1 \tag{3}$$

and the side-slip angle is

$$\alpha = \delta_i - (V + a_ir)/U \tag{4}$$

where δ_i is the wheel steering angle. We will regard λ and δ as the inputs to the model.

A linear description of the tire forces is given by

$$X = ZC_\lambda\lambda \tag{5a}$$
$$Y = ZC_\alpha\alpha = C_\alpha\left(\delta - (V + ar)/U\right) \tag{5b}$$

This description is accurate for small slips and slip angles, but otherwise the nonlinear characteristics of the tire need to be included. The yaw-control system will operate at the stability limits of the vehicle, with large

side-slips. Combining the linear tyre model (5) with the linear tractor model (2a) yields

$$E\frac{d}{dt}x = Ax + B_\lambda \lambda + B_\delta \delta \tag{6}$$

with $x = (V, r)^T$ and

$$E = \begin{bmatrix} m & mx \\ mx & I \end{bmatrix} \tag{7a}$$

$$A = \begin{bmatrix} -2(Z_f C_{\alpha,f} + Z_r C_{\alpha,r})/U & -(U^2 m + 2Z_f C_{\alpha,f} a_f - 2Z_r C_{\alpha,r} a_r)/U \\ -2(Z_f C_{\alpha,f} a_f - Z_r C_{\alpha,r} a_r)/U & -(mxU^2 + 2a_f^2 Z_f C_{\alpha,f} + 2a_r^2 Z_r C_{\alpha,r})/U \end{bmatrix} \tag{7b}$$

$$B_\delta = \begin{bmatrix} 2Z_f C_{\alpha,f} \\ 2Z_f C_{\alpha,f} a_f \end{bmatrix} \tag{7c}$$

$$B_\lambda = \begin{bmatrix} 0 & 0 & 0 & 0 \\ b_f Z_f C_{\lambda,f} & -b_f Z_f C_{\lambda,f} & b_r Z_r C_{\lambda,r} & -b_r Z_r C_{\lambda,r} \end{bmatrix} \tag{7d}$$

2.2 Tractor-Semitrailer Dynamics

Introduce the articulated tractor-semitrailer vehicle combination in Figure 4. In modelling the tractor-semitrailer dynamics it is more convenient

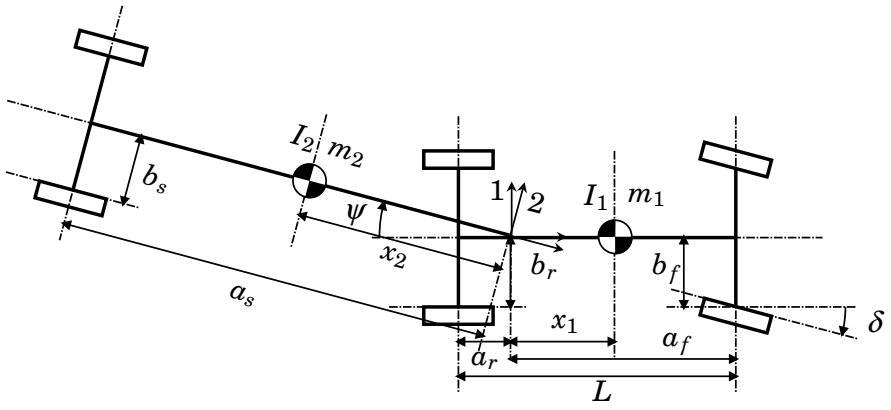

Figure 4 Geometry of the tractor-semitrailer vehicle combination.

to locate the origin at the hitch rather than in the CM. Introduce the state vector

$$\xi' = (U, V, r, \dot{\psi}, \psi)^T \tag{8}$$

where U and V are longitudinal and lateral velocity, r the yaw-rate, and $\dot{\psi}$ and ψ articulation angular velocity and angle. Introduce the inputs

as the front wheels steering angle δ, and the longitudinal wheel slips $\lambda = \left(\lambda_{fl}, \lambda_{fr}, \lambda_{rl}, \lambda_{rr}, \lambda_{sl}, \lambda_{sr}\right)^T$. Denote by $X_1(\xi', \delta, \lambda)$ and $Y_1(\xi', \delta, \lambda)$ the sum of longitudinal and lateral tyre forces acting on the tractor, and by $M_1(\xi', \delta, \lambda)$ their corresponding total moment. Let $X_2(\xi', \lambda)$,$Y_2(\xi', \lambda)$ and $M_2(\xi', \lambda)$ be defined equivalently for the semitrailer. The equations of motions can be written on matrix form as [GSC00]

$$H'(\xi')\frac{d\xi'}{dt} = F'(\xi') + G'(\xi', X_1(\cdot), Y_1(\cdot), M_1(\cdot), X_2(\cdot), Y_2(\cdot), M_2(\cdot)) \tag{9}$$

with

$$H'(\cdot) = \begin{bmatrix} m & 0 & -m_2 x_2 \sin\psi & -m_2 x_2 \sin\psi & 0 \\ 0 & m & m_1 x_1 + m_2 x_2 \cos\psi & m_2 x_2 \cos\psi & 0 \\ 0 & m_1 x_1 & I_1 & 0 & 0 \\ -m_2 x_2 \sin\psi & m_2 x_2 \cos\psi & I_2 & I_2 & 0 \\ 0 & 0 & 0 & 0 & 1 \end{bmatrix}, \tag{10a}$$

$$F'(\cdot) = \begin{bmatrix} mVr + m_1 r^2 x_1 + m_2 \left(r + \dot{\psi}\right)^2 x_2 \cos\psi \\ -mUr + m_2 \left(r + \dot{\psi}\right)^2 x_2 \sin\psi \\ -m_1 x_1 U r \\ -m_2 x_2 r \left(U \cos\psi + V \sin\psi\right) \\ \dot{\psi} \end{bmatrix} \tag{10b}$$

and

$$G'(\cdot) = \begin{bmatrix} X_1 + X_2 \cos\psi - Y_2 \sin\psi \\ Y_1 + X_2 \sin\psi + Y_2 \cos\psi \\ M_1 \\ M_2 \\ 0 \end{bmatrix} \tag{10c}$$

where $m = m_1 + m_2$.

We now introduce a linear model for constant longitudinal speed $U = U_0$, with the new state vector $\xi = (V, r, \dot{\psi}, \psi)$, at the stationary operating point $\xi_0 = (0, 0, 0, 0)$, $\delta_0 = 0$, $\lambda_0 = (0, 0, 0, 0, 0, 0)^T$ (free-rolling straight driving). Let H, F and G denote the portions of H', F' and G' corresponding to ξ. Then $F(\xi_0, \delta_0, \lambda_0) = 0$. Let $\Delta\xi = \xi - \xi_0$, $\Delta\delta = \delta - \delta_0$ and $\Delta\lambda = \lambda - \lambda_0$. Then

$$\begin{aligned} \frac{d}{dt}\Delta\xi \approx H(\xi_0)^{-1} \Bigg\{ F(\cdot)\Big|_0 + \left(\frac{\partial F(\cdot)}{\partial \xi} + \frac{\partial G(\cdot)}{\partial \xi} + \sum_k \frac{\partial G(\cdot)}{\partial f_k}\frac{\partial f_k(\cdot)}{\partial \xi}\right)\Bigg|_0 \Delta\xi + \\ \sum_k \frac{\partial G(\cdot)}{\partial f_k}\frac{\partial f_k(\cdot)}{\partial \delta}\Bigg|_0 \Delta\delta + \sum_k \frac{\partial G(\cdot)}{\partial f_k}\frac{\partial f_k(\cdot)}{\partial \lambda}\Bigg|_0 \Delta\lambda \Bigg\} \end{aligned} \tag{11}$$

with $\{f_k(\cdot)\} = \{X_1(\cdot), Y_1(\cdot), M_1(\cdot), X_2(\cdot), Y_2(\cdot), M_2(\cdot),\}$ and higher order terms neglected. This linear model is written on standard form as

$$\frac{d\xi}{dt} = A\xi + B_\delta \delta + B_\lambda \lambda \tag{12}$$

with

$$A = H(\xi_0)^{-1} \left(\frac{\partial F(\cdot)}{\partial \xi} + \frac{\partial G(\cdot)}{\partial \xi} + \sum_k \frac{\partial G(\cdot)}{\partial f_k} \frac{\partial f_k(\cdot)}{\partial \xi} \right) \Bigg|_0 \tag{13a}$$

$$B_\delta = H(\xi_0)^{-1} \sum_k \frac{\partial G(\cdot)}{\partial f_k} \frac{\partial f_k(\cdot)}{\partial \delta} \Bigg|_0 \tag{13b}$$

$$B_\lambda = H(\xi_0)^{-1} \sum_k \frac{\partial G(\cdot)}{\partial f_k} \frac{\partial f_k(\cdot)}{\partial \lambda} \Bigg|_0 \tag{13c}$$

With linear tyre models the tyre forces and moment for one wheel is described by

$$X = ZC_\lambda \lambda \tag{14a}$$

$$Y = ZC_\alpha \alpha = C_\alpha \left(\delta - \frac{V + ar}{U} \right) \tag{14b}$$

$$M = -bX + aY \tag{14c}$$

Inserted in (13) this yields the matrices of Figure 5.

It is also possible to linearize only the chassis dynamics, and combine it with a nonlinear tyre model. This yields

$$\frac{d}{dt}\Delta\xi \approx H(\xi_0)^{-1} \left\{ F(\xi) \Big|_0 + \left(\frac{\partial F(\cdot)}{\partial \xi} + \frac{\partial G(\cdot)}{\partial \xi} \right) \Bigg|_0 \Delta\xi + G(\xi_0, \cdot) \right\} \tag{15}$$

or

$$\frac{d}{dt}\xi = \bar{A}\xi + H(\xi_0)^{-1} G(\xi_0, \cdot) \tag{16}$$

with

$$\bar{A} = H(\xi_0)^{-1} \left(\frac{\partial F(\cdot)}{\partial \xi} + \frac{\partial G(\cdot)}{\partial \xi} \right) \Bigg|_0 = H(\xi_0)^{-1} \begin{bmatrix} 0 & -(m_1 + m_2)U & 0 & 0 \\ 0 & -m_1 x_1 U & 0 & 0 \\ 0 & m_2 x_2 U & 0 & 0 \\ 0 & 0 & 1 & 0 \end{bmatrix} \tag{17}$$

3. Nonlinear Tyre Models

The two most influential nonlinear properties of the tire adhesion forces in the context of yaw control is the saturation of the adhesion forces at large slips, and the effects of combined braking and cornering. Another nonlinear property is the adhesion forces dependence on the vertical load Z. Here it

$$
H(\xi_0) = \begin{bmatrix} m_1 + m_2 & m_1 x_1 - x_2 m_2 & -x_2 m_2 & 0 \\ m_1 x_1 & I_1 & 0 & 0 \\ -x_2 m_2 & I_2 & I_2 & 0 \\ 0 & 0 & 0 & 1 \end{bmatrix}
$$

$$
\left(\frac{\partial F(\cdot)}{\partial \xi} + \frac{\partial G(\cdot)}{\partial \xi} + \sum_k \frac{\partial G(\cdot)}{\partial f_k} \frac{\partial f_k(\cdot)}{\partial \xi} \right) \Bigg|_0 = \begin{bmatrix} -2(Z_f C_{\alpha,f} + Z_r C_{\alpha,r} + C_{\alpha,s} Z_s)/U & \cdots \\ -2(Z_f C_{\alpha,f} a_f - Z_r C_{\alpha,r} a_r)/U & \\ +2Z_s C_{\alpha,s} a_s/U & \\ 0 & \\ -(U^2 m_1 + U^2 m_2 + 2Z_f C_{\alpha,f} a_f - 2Z_r C_{\alpha,r} a_r - 2a_s Z_s C_{\alpha,s})/U & +2Z_s C_{\alpha,s} a_s/U \quad 2C_{\alpha,s} Z_s \\ -(m_1 x_1 U^2 + 2a_f^2 Z_f C_{\alpha,f} + 2a_r^2 Z_r C_{\alpha,r})/U & 0 \quad 0 \\ \cdots & -2C_{\alpha,s} Z_s a_s^2/U \quad -2a_s Z_s C_{\alpha,s} \\ -(-U^2 x_2 m_2 + 2C_{\alpha,s} Z_s a_s^2)/U & 1 \quad 0 \\ 0 & \end{bmatrix}
$$

$$
\sum_k \frac{\partial G(\cdot)}{\partial f_k} \frac{\partial f_k(\cdot)}{\partial \delta} \Bigg|_0 = \begin{bmatrix} 2Z_f C_{\alpha,f} & 2Z_f C_{\alpha,f} a_f & 0 & 0 \end{bmatrix}
$$

$$
\sum_k \frac{\partial G(\cdot)}{\partial f_k} \frac{\partial f_k(\cdot)}{\partial \lambda} \Bigg|_0 = \begin{bmatrix} 0 & 0 & 0 & 0 & 0 & 0 & 0 \\ b_f Z_f C_{\lambda,f} & -b_f Z_f C_{\lambda,f} & b_r Z_r C_{\lambda,r} & -b_r Z_r C_{\lambda,r} & 0 & 0 & 0 \\ 0 & 0 & 0 & 0 & 0 & b_s Z_s C_{\lambda,s} & -b_s Z_s C_{\lambda,s} \\ 0 & 0 & 0 & 0 & 0 & 0 & 0 \end{bmatrix}
$$

Figure 5 Matrices for expressions (13).

is assumed that the adhesion forces depend linearly on Z, and we denote X/Z and Y/Z as adhesion coefficients. There is a vast number of tire models that capture these phenomena. In analysing handling dynamics of a vehicle analytically it is desired to have an analytical simplistic model, while a more complex model may be used in simulations.

3.1 Saturation of Adhesion Forces

The saturation characteristics for a real tire are shown in Figure 6. We

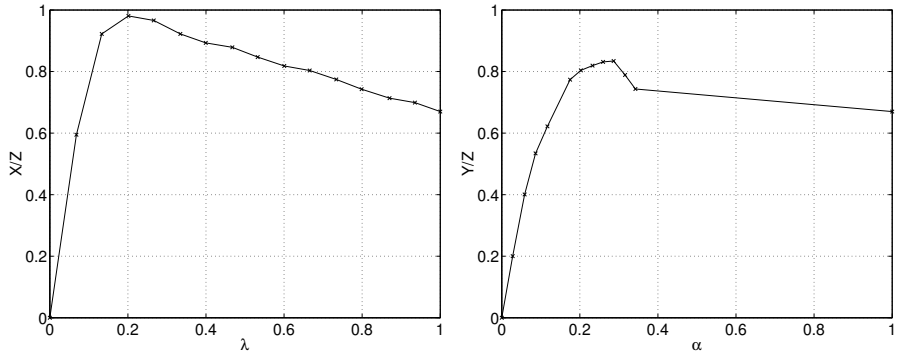

Figure 6 Experimental tire adhesion coefficients at pure braking and pure cornering. The last data value for the lateral adhesion coefficient is estimated as being equal to the longitudinal adhesion coefficient for $\lambda = 1$. The experimental data is obtained from Volvo Truck Corporation [Edl91].

need tire models to capture these saturations of the adhesion coefficients. Introduce the saturation function as

$$\text{sat}(x) = \begin{cases} x, & |x| < 1 \\ \text{sgn}(x), & \text{otherwise} \end{cases} \tag{18}$$

At pure braking ($\alpha = 0$) the nonlinear tire characteristics may be approximated by

$$X = ZC_\lambda \lambda^* \,\text{sat}\left(\lambda/\lambda^*\right) \tag{19}$$

$$Y = 0 \tag{20}$$

At pure cornering ($\lambda = 0$) it may be approximated as

$$X = 0 \tag{21}$$

$$Y = ZC_\alpha \alpha^* \,\text{sat}\left(\alpha/\alpha^*\right) \tag{22}$$

In reality the contact forces often decreases with increasing slip in the nonlinear region. This may lead to destabilizing effects that are not captured by this approximation. The model is compared with experimental data in Figure 7.

3.2 Combined Braking and Cornering

At combined braking and cornering the adhesion coefficients are reduced compared to pure braking and pure cornering. This is illustrated for a real tire in Figure 8. A main issue for more advanced tire models is to reproduce this property. In [BB00] the authors list a number of criteria that should be fulfilled by a model for combined braking and cornering:

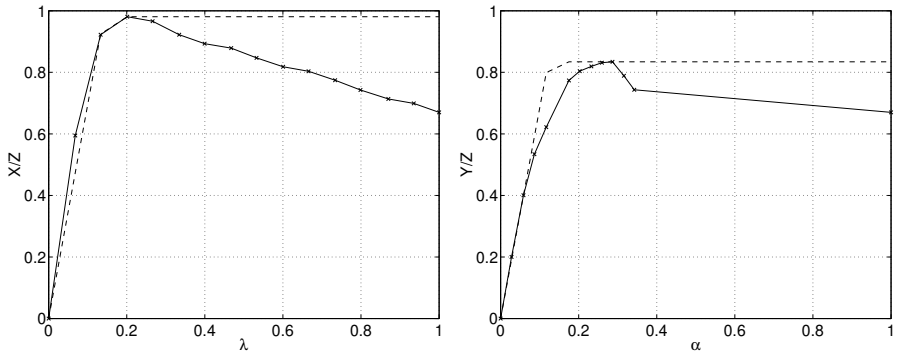

Figure 7 Saturated linear adhesion forces (dashed) compared to experimental data (solid). The experimental data is obtained from Volvo Truck Corporation [Edl91].

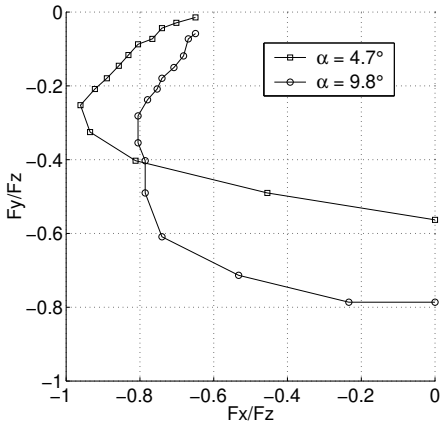

Figure 8 Experimental tire adhesion coefficients at combined braking and cornering for two fixed α and varying λ. The experimental data is obtained from Volvo Truck Corporation [Edl91].

1. The combined longitudinal force component $X(\alpha, \lambda)$ should approach the longitudinal force at pure braking $X_0(\lambda)$ as $\alpha \to 0$.
2. The combined lateral force component $Y(\alpha, \lambda)$ should approach the lateral force at pure cornering $Y_0(\alpha)$ as $\lambda \to 0$.
3. The combined adhesion force $\sqrt{X^2(\alpha, \lambda) + Y^2(\alpha, \lambda)}$ must be limited.
4. The combined tire forces $X(\alpha, \lambda)$, $Y(\alpha, \lambda)$ must agree at least approximately with experimental results.
5. The combined tire force $\sqrt{X^2(\alpha, \lambda) + Y^2(\alpha, \lambda)}$ should produce a force equal to μZ in a direction opposite to the velocity vector for a locked wheel skid ($\lambda = 1$) for any α.

It is interesting to investigate these properties for the linear tire model (5). Properties 1. and 2. are trivially fulfilled. The longitudinal velocity of the tire surface relative the road is $R_w\omega - U = \lambda U$. Thus the tire surface has the velocity vector $[\lambda U, V]^T$. The adhesion force vector $[X, Y]$ is $[C_\lambda \lambda, C_\alpha \alpha]$ for the linear tire model. Property 5. implies that $X/Y = U/V$ when $\lambda = 0$. For the linear model $X/Y = (C_\lambda \lambda / C\alpha\alpha) = (C_\lambda \lambda U)/(C_\alpha V) \to$

$(C_\lambda/C_\alpha)(U/V)$ as $\lambda \to 1$ (for small α). For $C_\alpha \approx C_\lambda$ the linear model thus produce adhesion forces with appropriate direction. This motivates a simple model for combined braking and cornering forces based on the linear tire model (5), modified to include limitation according to Property 3., such that Property 4. holds. Such a model is described in the next section.

3.3 Slip Saturation Model

A wellknown family of tire models for combined braking and cornering are based on ellipsoidal constraints like

$$\left(\frac{X}{ZC_\lambda\lambda^*}\right)^2 + \left(\frac{Y}{ZC_\alpha\alpha^*}\right)^2 \leq 1 \tag{23}$$

In these models the tire forces may be regarded as generated by *effective* slip components (λ', α') as $X = ZC_\lambda\lambda'$ and $Y = ZC_\alpha\alpha'$ where $(\lambda', \alpha') = \mathrm{sat}_{(\lambda^*,\alpha^*)}(\lambda, \alpha)$. The ellipsoidal saturation $\mathrm{sat}_{(a,b)}$ function is defined as

$$\mathrm{sat}_{(a,b)}(x,y) = \begin{cases} (x,y), & (x/a)^2 + (y/b)^2 \leq 1 \\ (x',y') : x'/y' = x/y,\ (x/a)^2 + (y/b)^2 = 1, & \text{otherwise} \end{cases} \tag{24}$$

Here the tire nonlinearities may be regarded as a two-dimensional ellipsoidal saturation.

The constants λ^* and α^* are dependent on surface and tyre conditions. Typical values are $\lambda^* \approx 0.2$ for dry asphalt, $\lambda^* \approx 0.1$ for wet asphalt, and $\lambda^* \approx 0.05$ for snow.

The slip saturation model is compared with experimental data in Figure 9. For large slips the model does not capture the decreasing adhesion coefficient.

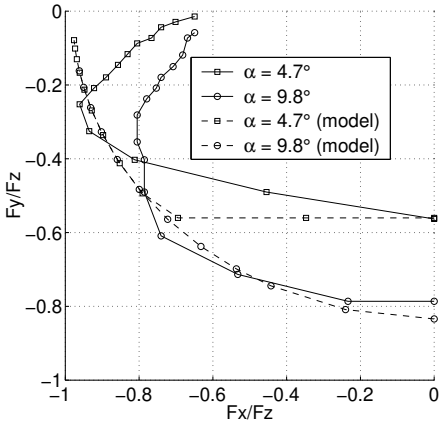

Figure 9 Slip saturation model and experimental adhesion coefficients at combined braking and cornering for two fixed α and varying λ. The experimental data is obtained from Volvo Truck Corporation [Edl91].

3.4 Friction Ellipse Model

One commonly used simple friction ellipse tyre model has the form

$$\left(\frac{X(\lambda, Z)}{X_{\max}}\right)^2 + \left(\frac{Y}{Y(\alpha, Z)}\right)^2 = 1 \tag{25}$$

This expression gives the resulting cornering force Y at a given longitudinal force $X(\lambda, Z)$, where $Y(\alpha, Z)$ is the cornering force in absence of any longitudinal force. Rearrangement results in

$$Y = Y(\alpha, Z)\sqrt{1 - \left(\frac{X(\lambda, Z)}{X_{\max}}\right)^2} \tag{26}$$

Using $X = ZC_\lambda \lambda^* \operatorname{sat}(\lambda/\lambda^*)$, $Y = ZC_\alpha \alpha^* \operatorname{sat}(\alpha/\alpha^*)$, and $X_{\max} = ZC_\lambda \lambda^*$ gives

$$Y = ZC_\alpha \alpha^* \operatorname{sat}(\alpha/\alpha^*)\sqrt{1 - \operatorname{sat}(\lambda/\lambda^*)^2} \tag{27}$$

3.5 Slip Circle Model

The *slip circle* model [SPP96] is a generic tyre model for combined braking and cornering based on models of pure braking and cornering. Introduce the dimensionless slip variable s

$$s \equiv \sqrt{\lambda^2 + \sin^2 \alpha} \tag{28}$$

(It is common to describe the side-slip with the dimensionless entity $\sin\alpha$ instead of α. For small α the difference is negligable.) Define the slip angle β as

$$\tan\beta \equiv \frac{\sin\alpha}{\lambda} \tag{29}$$

The tyre force is asssumed to be counterdirected to the slip vector described by s and β.

Now introduce the pure cornering and braking mappings from slips to tyre forces $f : \lambda \mapsto X$ and $g : \alpha \mapsto Y$. In the slip cirlce model the magnitude of the combined tyre force is now described as

$$F = f(s)\cos^2\beta + g(s)\sin^2\beta = \left(f(s)\lambda^2 + g(s)\sin^2\alpha\right)/s \tag{30}$$

It is seen that pure cornering and braking are restored for $\beta = 0$ and $\beta = \pi/2$. For other β the combined tyre forces lies on a curve that is "close" to an ellipse. The slip circle model is compared with experiments in Figure 10.

4. Analysis of Vehicle Dynamics

In this section the combination of the linear tractor dynamics of Section 2.1 and the slip saturation model of Section 3.3 will be analysed.

4.1 Feedback Interpretation

With saturated tire forces the tractor dynamics become

$$m\dot{V} = -mUr + Y' \tag{31}$$

$$J\dot{r} = bX' + aY' \tag{32}$$

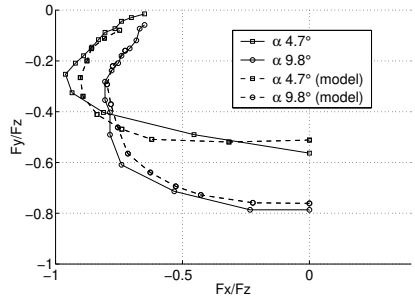

Figure 10 Slip-circle model and experimental adhesion coefficients at combined braking and cornering for two fixed α and varying λ. The experimental data is obtained from Volvo Truck Corporation [Edl91].

Hence the linear systems dynamics reduce to a double integrator at saturation. This may be viewed as an internal feedback loop that is broken at saturation.

Introduce the state vector $x = (V, r)^T$, the input signal vector $u = (\lambda, \delta)^T$, the internal feedback gain

$$K = \begin{bmatrix} 0 & 0 \\ -1/JU & -a/JU \end{bmatrix}, \tag{33}$$

and the system matrices

$$A = \begin{bmatrix} 0 & -U \\ 0 & 0 \end{bmatrix}, \qquad B = \begin{bmatrix} 0 & C_\alpha/m \\ bZC_\lambda/J & aZC_\alpha/J \end{bmatrix}. \tag{34}$$

Now the system dynamics may be described by the block diagram in Figure 11. The two dimensional saturation function brakes the linear feedback

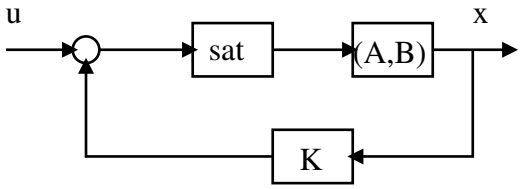

Figure 11 Block diagram of vehicle

loop. The resulting dynamics then is a double integrator driven by the nonlinear feedback introduced by the saturation function.

4.2 Saturation Region

In the saturation region the tyre forces are described by $X = ZC_\lambda \lambda'$, $Y = ZC_\alpha \alpha'$, with $(\lambda', \alpha') = \mathrm{sat}_{(\lambda^*, \alpha^*)}(\lambda, \alpha)$. This implies that

$$\frac{\lambda}{\alpha} = \frac{\lambda'}{\alpha'} \tag{35}$$

and

$$\left(\frac{\lambda'}{\lambda^*}\right)^2 + \left(\frac{\alpha'}{\alpha^*}\right)^2 = 1. \tag{36}$$

Now let us investigate what control authority we have with the slip input λ under these conditions. We see that

$$\lambda' = \frac{\alpha'}{\alpha}\lambda \tag{37}$$

The factor α'/α is smaller for large side-slips ($\alpha' \leq \alpha^*$), i.e. where the vehicle is far outside the linear region. Large side-slip thus reduces the longitudinal control authority.

Inserting (37) in (36) results in

$$\left(\frac{\alpha'\lambda}{\alpha\lambda^*}\right)^2 + \left(\frac{\alpha'}{\alpha^*}\right)^2 = 1. \tag{38}$$

or

$$\alpha' = \frac{\alpha}{\sqrt{\left(\frac{\lambda}{\lambda^*}\right)^2 + \left(\frac{\alpha}{\alpha^*}\right)^2}} = \alpha^* - \frac{1}{2}\frac{\alpha^{*3}}{(\alpha\lambda^*)^2}\lambda^2 + O(\lambda^4) \tag{39}$$

and consequently

$$\lambda' = \frac{\lambda}{\sqrt{\left(\frac{\lambda}{\lambda^*}\right)^2 + \left(\frac{\alpha}{\alpha^*}\right)^2}} = \alpha^* - \frac{1}{2}\frac{\alpha^{*3}}{(\alpha\lambda^*)^2}\lambda^2 + O(\lambda^4) \tag{40}$$

This means the side forces reduce quadratically with small braking actions. A more complete picture of how braking actions affect the side forces is shown in Figure 12. There it is shown how the effective side-slip is reduced with increasing λ for different side-slips α. It is seen in the diagram that for

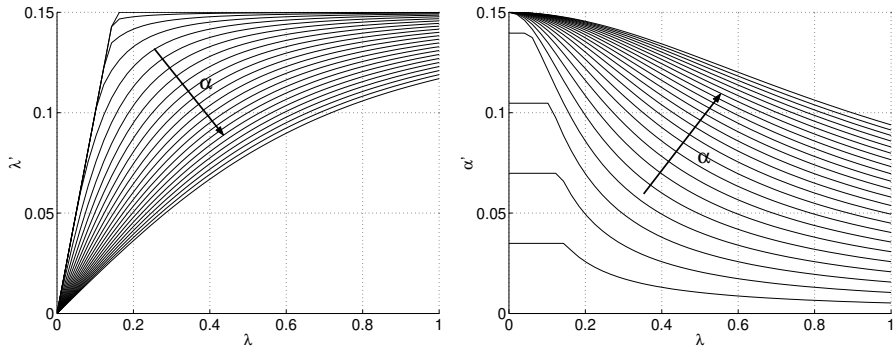

Figure 12 Effect of changing λ (braking) on effective longitudinal slip λ' and effective side slip α' (side force) for side slips $\alpha \in [0, 46^\circ]$ (grid size 2°). The saturation limits are set to $\lambda^* = \alpha^* = 0.15$.

small side-slips the effective side-slip is reduced significantly when braking, while for large side-slips the effect is less.

A summary of this investigation is that for small side-slips in the saturated region we have control authority with the brakes, but the braking action reduce the side forces significantly, which destabilizes the vehicle. At larger side-slips the control authority is reduced, while also the effect of braking on the side forces are less. Simply stated: we have lost control of the vehicle. Intuitively all this can be understood from Figure 13, where the saturation limit is shown together with slips and effective slips.

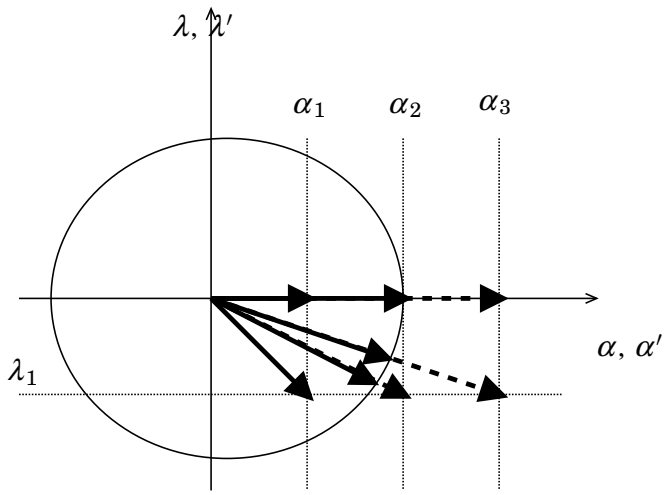

Figure 13 Effects of braking on effective slips. The same braking action λ_1 is applied at three different side-slips α: $\alpha_1 < \alpha^*$, $\alpha_2 = \alpha^*$, $\alpha_3 > \alpha^*$

4.3 Linear Region

The linear region for one wheel is characterized by

$$\left(\frac{\lambda}{\lambda^*}\right)^2 + \left(\frac{\alpha}{\alpha^*}\right)^2 \leq 1 \tag{41}$$

or

$$\left(\frac{\lambda}{\lambda^*}\right)^2 + \left(\frac{\delta - (V + ar)/U}{\alpha^*}\right)^2 \leq 1 \tag{42}$$

This is a linear inequality in the state-space (V, r) depending on steering and braking action δ and λ.

$$U\left(\delta - \alpha^*\sqrt{1 - \left(\frac{\lambda}{\lambda^*}\right)^2}\right) \leq V + ar \leq U\left(\delta + \alpha^*\sqrt{1 - \left(\frac{\lambda}{\lambda^*}\right)^2}\right) \tag{43}$$

The region is a band that gets smaller with increasing braking action, and that translates with the steering action. An example is shown in Figure 14. Including multiple wheels the total linear region is the cut of multiple such regions.

4.4 Disturbance Interpretation

Regard the vehicle dynamics

$$m\dot{V} = -mUr + Y \tag{44}$$

$$J\dot{r} = -bX + aY \tag{45}$$

together with the slip-saturation tyre model

$$(\lambda', \alpha') = \mathrm{sat}_{(\lambda^*, \alpha^*)}(\lambda, \alpha) \tag{46}$$

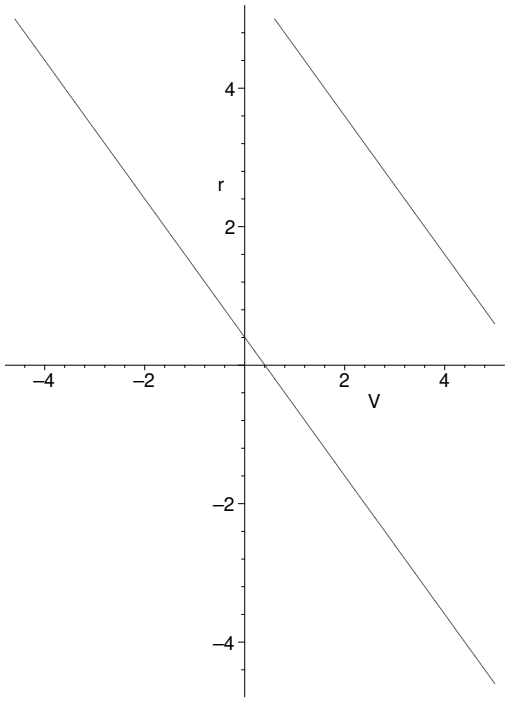

Figure 14 The linear region for $\lambda = 0.05$, $\delta = 0.1$, $\lambda^* = 0.1$ and $\alpha^* = 0.1$.

where $\alpha = \delta - (V + ar)/U$ and

$$X = C_\lambda \lambda' = C_\lambda \lambda + C_\lambda \tilde{\lambda} \tag{47}$$
$$Y = C_\alpha \alpha' = C_\alpha \alpha + C_\alpha \tilde{\alpha} \tag{48}$$

with $\tilde{\lambda} = \lambda' - \lambda$ and $\tilde{\alpha} = \alpha' - \alpha$ Thus

$$m\dot{V} = -\frac{C_\alpha}{U} V - \left(mU + \frac{C_\alpha a}{U} \right) r + C_\alpha \delta + C_\alpha \tilde{\alpha} \tag{49}$$
$$J\dot{r} = -\frac{C\alpha a}{U} V - \frac{C_\alpha a^2}{U} r + aC_\alpha \delta - bC_\lambda \lambda - bC_\lambda \tilde{\lambda} + aC_\alpha \tilde{\alpha} \tag{50}$$

Hence the deviation frm the linear behaviour may be regarded as disturbances $\tilde{\lambda}$ and $\tilde{\alpha}$.

4.5 Piecewise Affine Model

By formulating the vehicle dynamics as a piecewise affine model it is possible to use piecewise-affine theory [Joh99] to investigate stability properties. This may be used to find bounds on stabilizable regions in the state-space, which define performance limits on yaw-control algorithms. At cornering with moderate braking intervention it is reasonable to regard a tyre model with nonlinear saturating lateral tire forces, and linear longitudinal tyre forces. The tyre forces may then be modelled as

$$X = ZC_\lambda \lambda \tag{51a}$$
$$Y = ZC_\alpha \alpha^* \operatorname{sat}\left(\alpha/\alpha^*\right) \tag{51b}$$

where λ is the longitudinal slip, and α the side slip. The longitudinal tyre forces at the front/rear, left/right wheels are

$$X_{fl} = Z_f C_\lambda \lambda_{fl} \tag{52a}$$
$$X_{fr} = Z_f C_\lambda \lambda_{fr} \tag{52b}$$
$$X_{rl} = Z_r C_\lambda \lambda_{rl} \tag{52c}$$
$$X_{rr} = Z_r C_\lambda \lambda_{rr} \tag{52d}$$

The front and rear side-slips are

$$\alpha_{fl} \equiv \alpha_{fr} = \delta - \left(V + a_f r\right)/U \tag{53a}$$
$$\alpha_{rl} \equiv \alpha_{rr} = -\left(V - a_r r\right)/U \tag{53b}$$

where δ is the drivers steering wheel input. The corresponding tyre forces are

$$Y_f = 2Z_f C_\alpha \alpha^* \operatorname{sat}\left(\alpha_f/\alpha^*\right) \tag{54a}$$
$$Y_r = 2Z_r C_\alpha \alpha^* \operatorname{sat}\left(\alpha_r/\alpha^*\right) \tag{54b}$$

where the left and right wheels have been lumped together. The moment acting on the car from the tyre forces is

$$M = a_f Y_f - a_r Y_r + bZ_f(\lambda_{fl} - \lambda_{fr}) + bZ_r(\lambda_{rl} - \lambda_{rr}) \tag{55}$$

introduce $\lambda_f = \lambda_{fl} - \lambda_{fr}$, $\lambda_r = \lambda_{rl} - \lambda_{rr}$. The equations of motion for a car with constant longitudinal velocity U become

$$m\dot{V} = -mUr + Y_f + Y_r \tag{56a}$$
$$J\dot{r} = a_f Y_f - a_r Y_r + bZ_f C_\lambda \lambda_f + bZ_r C_\lambda \lambda_r \tag{56b}$$

where V is the lateral velocity, and r the yaw rate. (Some may find it more convenient to state the equations of motion in the side-slip variable $\beta = U/V$ instead of the lateral velocity V. This is just a scaling.) The linear regions for the front and rear tyres are

$$U\left(\delta - \alpha^*\right) \underset{f^-}{\leq} V + a_f r \underset{f^+}{\leq} U\left(\delta + \alpha^*\right) \tag{57a}$$
$$-U\alpha^* \underset{r^-}{\leq} V - a_r r \underset{r^+}{\leq} U\alpha^* \tag{57b}$$

where f^-, f^+, r^-, r^+ are labels on the inequalities. This may be expressed as the piecewise affine model

$$\dot{x} = A_i x + B_i u + b_i \tag{58}$$

with $x = [\delta, \lambda_f, \lambda_r]$, $u = [\delta, \lambda_f, \lambda_r]$, and A_i, B_i, b_i defined as follows:

0. *No inequalities violated*

$$\begin{aligned} A_0 &= \begin{bmatrix} -\frac{2C_\alpha(Z_f+Z_r)}{mU} & -\frac{mU^2+2C_\alpha(a_f Z_f - a_r Z_r)}{mU} \\ -\frac{2C_\alpha(a_f Z_f - a_r Z_r)}{JU} & -\frac{2C_\alpha(a_f^2 Z_f + a_r^2 Z_r)}{JU} \end{bmatrix}, \\ B_0 &= \begin{bmatrix} \frac{2Z_f C_\alpha}{m} & 0 & 0 \\ \frac{2a_f Z_f C_\alpha}{J} & \frac{bZ_f C_\lambda}{J} & \frac{bZ_r C_\lambda}{J} \end{bmatrix}, \qquad b_0 = \begin{bmatrix} 0 \\ 0 \end{bmatrix} \end{aligned} \tag{59a}$$

1. f^- *violated*

$$\begin{aligned} A_1 &= \begin{bmatrix} -\frac{2C_\alpha Z_r}{mU} & -\frac{mU^2-2C_\alpha a_r Z_r}{mU} \\ \frac{2C_\alpha a_r Z_r}{JU} & -\frac{2C_\alpha a_r^2 Z_r}{JU} \end{bmatrix}, \\ B_1 &= \begin{bmatrix} 0 & 0 & 0 \\ 0 & \frac{bZ_f C_\lambda}{J} & \frac{bZ_r C_\lambda}{J} \end{bmatrix}, \qquad b_1 = \begin{bmatrix} -\frac{2Z_f C_\alpha \alpha^*}{m} \\ -\frac{2a_f Z_f C_\alpha \alpha^*}{J} \end{bmatrix} \end{aligned} \tag{59b}$$

2. f^+ *violated*

$$\begin{aligned} A_2 &= \begin{bmatrix} -\frac{2C_\alpha Z_r}{mU} & -\frac{mU^2-2C_\alpha a_r Z_r}{mU} \\ \frac{2C_\alpha a_r Z_r}{JU} & -\frac{2C_\alpha a_r^2 Z_r}{JU} \end{bmatrix}, \\ B_2 &= \begin{bmatrix} 0 & 0 & 0 \\ 0 & \frac{bZ_f C_\lambda}{J} & \frac{bZ_r C_\lambda}{J} \end{bmatrix}, \qquad b_2 = \begin{bmatrix} \frac{2Z_f C_\alpha \alpha^*}{m} \\ \frac{2a_f Z_f C_\alpha \alpha^*}{J} \end{bmatrix} \end{aligned} \tag{59c}$$

3. r^- *violated*

$$\begin{aligned} A_3 &= \begin{bmatrix} -\frac{2C_\alpha Z_f}{mU} & -\frac{mU^2+2C_\alpha a_f Z_f}{mU} \\ -\frac{2C_\alpha a_f Z_f}{JU} & -\frac{2C_\alpha a_f^2 Z_f}{JU} \end{bmatrix}, \\ B_3 &= \begin{bmatrix} \frac{2Z_f C_\alpha}{m} & 0 & 0 \\ \frac{2a_f Z_f C_\alpha}{J} & \frac{bZ_f C_\lambda}{J} & \frac{bZ_r C_\lambda}{J} \end{bmatrix}, \qquad b_3 = \begin{bmatrix} -\frac{2Z_r C_\alpha \alpha^*}{m} \\ \frac{2a_r Z_r C_\alpha \alpha^*}{J} \end{bmatrix} \end{aligned} \tag{59d}$$

4. r^+ *violated*

$$\begin{aligned} A_4 &= \begin{bmatrix} -\frac{2C_\alpha Z_f}{mU} & -\frac{mU^2+2C_\alpha a_f Z_f}{mU} \\ -\frac{2C_\alpha a_f Z_f}{JU} & -\frac{2C_\alpha a_f^2 Z_f}{JU} \end{bmatrix}, \\ B_4 &= \begin{bmatrix} \frac{2Z_f C_\alpha}{m} & 0 & 0 \\ \frac{2a_f Z_f C_\alpha}{J} & \frac{bZ_f C_\lambda}{J} & \frac{bZ_r C_\lambda}{J} \end{bmatrix}, \qquad b_4 = \begin{bmatrix} \frac{2Z_r C_\alpha \alpha^*}{m} \\ -\frac{2a_r Z_r C_\alpha \alpha^*}{J} \end{bmatrix} \end{aligned} \tag{59e}$$

5. f^-, r^- *violated*

$$\begin{aligned} A_5 &= \begin{bmatrix} 0 & -U \\ 0 & 0 \end{bmatrix}, \\ B_5 &= \begin{bmatrix} 0 & 0 & 0 \\ 0 & \frac{bZ_f C_\lambda}{J} & \frac{bZ_r C_\lambda}{J} \end{bmatrix}, \qquad b_5 = \begin{bmatrix} -\frac{2(Z_r+Z_f) C_\alpha \alpha^*}{m} \\ \frac{2(a_r Z_r - a_f Z_f) C_\alpha \alpha^*}{J} \end{bmatrix} \end{aligned} \tag{59f}$$

6. f^-, r^+ *violated*

$$\begin{aligned} A_6 &= \begin{bmatrix} 0 & -U \\ 0 & 0 \end{bmatrix}, \\ B_6 &= \begin{bmatrix} 0 & 0 & 0 \\ 0 & \frac{bZ_f C_\lambda}{J} & \frac{bZ_r C_\lambda}{J} \end{bmatrix}, \qquad b_6 = \begin{bmatrix} \frac{2(Z_r-Z_f) C_\alpha \alpha^*}{m} \\ -\frac{2(a_r Z_r + a_f Z_f) C_\alpha \alpha^*}{J} \end{bmatrix} \end{aligned} \tag{59g}$$

7. f^+, r^- *violated*

$$A_7 = \begin{bmatrix} 0 & -U \\ 0 & 0 \end{bmatrix},$$
$$B_7 = \begin{bmatrix} 0 & 0 & 0 \\ 0 & \frac{bZ_f C_\lambda}{J} & \frac{bZ_r C_\lambda}{J} \end{bmatrix}, \qquad b_7 = \begin{bmatrix} -\frac{2(Z_r - Z_f)C_\alpha \alpha^*}{m} \\ \frac{2(a_r Z_r + a_f Z_f)C_\alpha \alpha^*}{J} \end{bmatrix} \tag{59h}$$

8. f^+, r^+ *violated*

$$A_7 = \begin{bmatrix} 0 & -U \\ 0 & 0 \end{bmatrix},$$
$$B_7 = \begin{bmatrix} 0 & 0 & 0 \\ 0 & \frac{bZ_f C_\lambda}{J} & \frac{bZ_r C_\lambda}{J} \end{bmatrix}, \qquad b_7 = \begin{bmatrix} \frac{2(Z_r + Z_f)C_\alpha \alpha^*}{m} \\ -\frac{2(a_r Z_r - a_f Z_f)C_\alpha \alpha^*}{J} \end{bmatrix} \tag{59i}$$

Introduce $B_{\delta i} = (B_i)_{1..2,1}$ and $B_{\lambda i} = (B_i)_{1..2,2..3}$. The desired trajectory x_r for the vehicle is determined by the drivers steering wheel input δ and the linear model $(A_0, B_{\delta 0}, B_{\lambda 0}, b_0)$ as $x_r = -A_0^{-1} B_{\delta 0} \delta$. Determine a feedback law $u = h(x)$ with $u = [\lambda_f, \lambda_r]$ to solve the tracking problem.

5. Control Strategies

The majority of published work on AYC presents controllers based on Linear Quadratic control theory. Since the desired vehicle behaviour is most naturally expressed as reference state-trajectories, and there are methods to reconstruct the vehicle state, this is a natural approach. This study will also focus on LQ control. Most previous work used the desired moment to apply on the vehicle as a controller output. This moment is then mapped to desired slips or tire forces at the individual wheels. This results in a single output controller. In this study we will try to use the left/right wheel-slip difference at each axle as controller outputs. This results in a 2-output controller for the tractor vehicle, and a 3-output controller for the tractor-semitrailer vehicle.

The situations where control intervention is desireable are for a tractor: understeering and oversteering, and for a tractor-semitrailer combination: understeering, oversteering/jackknifing and trailer-swing.

The controller designs will be based on the disturbance interpretation of Section 4.4. That means the vehicle behaviour is assumed to be linear within the adhesion limit. At the adhesion limits the nonlinear effects are regarded as disturbances that can be rejected by the controllers. This assumption may be questioned, since the nonlinear effect actually is a structural change of the dynamics since the internal stabilizing feedback is broken, see Section 4.1.

The LQ-controllers minimize the cost function

$$J = \int (x - x_r)^T Q (x - x_r) + \lambda^T R \lambda \, dt \tag{60}$$

The weighting matrices Q and R is chosen as to trade-off between tracking errors in side-slip, yaw-rate, articulation-velocity and articulation angle, and the energy applied in control interventions. These are the tuning

parameters of the controller. The controller is of the form

$$u = -L(x - x_r) \tag{61}$$

with L being a constant gain matrix. Linear Quadratic control theory is described in [ÅW97].

The linear models (61–7) and (13a–13) will be used for controller design for the tractor and tractor with semi-trailer vehicles respectively. In the validations the linear dynamics (2a) and (16–17) will be used together with the slip-saturation tire model (23–24).

5.1 Reference trajectories

The desired reference trajectories are generated from the drivers steering wheel input, and the linear dynamics of the vehicle. The motivation for this is that the driver recognizes the linear behavior, and he/she will more likely manage to handle the vehicle if it behaves linearly. One possible reference trajectory is to use the steady-state gain of the linear model

$$x_r = -A^{-1}B_\delta\delta \tag{62}$$

A less realistic approach is taken here, where the linear models simply are simulated in parallell with the controllers, and the simulation outputs are used as references.

$$\frac{d}{dt}x_r = Ax_r + B_\delta\delta \tag{63}$$

5.2 Control Signals

Introspection of the input gain matrices B_λ reveals that the left and right wheels have equal gains with opposite signs. This means that the left and right input slips (λ_l, λ_r) on one axle can be treated as one aggregate slip signal λ. It is only possible to apply control in one direction at each wheel by braking ($\lambda_l < 0$, $\lambda_r < 0$). But mapping negative control signals $\lambda < 0$ to the right wheel as $\lambda_r = \lambda$ and positive control signals $\lambda > 0$ on the left wheel $\lambda_l = -\lambda$ gives in effect control in both directions.

It would be possible to design controllers that use braking on all axles simultaneously. This would mean designing controllers with the weights

$$Q = \text{diag}\left[Q_V, Q_r\right] \qquad R = \text{diag}\left[\lambda_f, \lambda_r\right] \tag{64}$$

for the tractor vehicle, and

$$Q = \text{diag}\left[Q_V, Q_r, Q_{\dot{\psi}}, Q_\psi\right] \qquad R = \text{diag}\left[\lambda_f, \lambda_r, \lambda_s\right] \tag{65}$$

for the tractor-semitrailer combination vehicle. This approach was tried, but performed inferiorly compared to controller that limited the control action to one tractor axle at the time. The mapping of control on front, rear and semitrailer axles depends on the nonlinear characteristics of the tires. In a linear system it would be mostly efficient to apply control on all inputs simultaneously. For the vehicles the nonlinear effects of the tires need to taken into account. The investigation in Section 4.2 showed that the lateral adhesion forces decrease with increased longitudinal slip. It is therefore not

appropriate to apply braking action on a wheel at the adhesion limit which has a stabilizing lateral adhesion force. At oversteering the rear axle is at the adhesion limits, and at understeering the front axle is at the limit. Therefore control on the front axle is used at oversteering and the rear axle at understeering. This strategy also gives additional stabilization in that the lost lateral force due to braking gives additional moment in the desired direction. The result is controllers with the weights en as

$$Q_f = \text{diag}\,[Q_V, Q_r] \qquad R_f = \lambda_f \tag{66a}$$
$$Q_r = \text{diag}\,[Q_V, Q_r] \qquad R_r = \lambda_r \tag{66b}$$
$$\tag{66c}$$

for the tractor vehicle, and

$$Q_f = \text{diag}\left[Q_V, Q_r, Q_{\dot{\psi}}, Q_\psi\right] \qquad R_f = \lambda_f \tag{67a}$$
$$Q_r = \text{diag}\left[Q_V, Q_r, Q_{\dot{\psi}}, Q_\psi\right] \qquad R_r = \lambda_r \tag{67b}$$
$$Q_s = \text{diag}\left[Q_V, Q_r, Q_{\dot{\psi}}, Q_\psi\right] \qquad R_s = \lambda_s \tag{67c}$$
$$\tag{67d}$$

for the tractor-semitrailer combination vehicle. This means two controllers (front/rear axles) for the tractor vehicle, where at most one is active at any time. For the tractor-semitrailer this means three controllers (front/rear/-semitrailer axles), where at most one of the front and rear axle controllers is active at any time, and the semitrailer axle controller may be active at any time. Other strategies are also possible.

For detection of oversteer or understeer it has been noted that the following invariants hold, with $\Delta x = x - x_r$:

	Oversteering	*Understeering*
$V\Delta V$	$-$	$+$
$r\Delta r$	$-$	$+$

In simulations it was observed that $V\Delta V$ gave better performance as detector. Using $r\Delta r$ often resulted in fast switching of the control between front and rear wheels.

With the assumption that the wheels are equipped with ABS the longitudinal slip is constrained to $|\lambda| \leq \lambda^*$. In this study the slip was instead limited $\lambda < 1$, with wheel lock as upper limit. This may not be so wise for a linear control strategy, since large λ gives larger nonlinear effects on lateral adhesion. However, since the front/rear control mapping is chosen such that the nonlinear effect helps stabilization it may be still be appropriate. The effect of this limit has not been studied further here.

5.3 State measurements

It is assumed that the state is available for feedback. Methods for reconstructing the state from sensor measurements is out of scope of this work.

6. Results

The controller and the controlled systems described in the previous sections was implemented and simulated in Matlab/Simulink. A number of

different configurations, scenarios and controllers have been examined. It should be emphasized that tuning efforts has been kept to a minimum, and that the results by no means should be regarded as the best possible. This study rather aims at finding characteristics of the different control strategies. Results of the simulations are presented in diagrams in Appendix A.

The scenarios that have been studied are presented in the subsections below toghether with discussions on the results. The vehicle parameters that have been used are shown in Table 1. Different controllers have been used in the scenarios as described in the corresponding subsections. Steering input δ, vehicle tire parameters (C_α, $C\lambda$) and road surface parameters (α^*, λ^*) have been chosen for each scenario such that the effect to study appears.

Parameter	*Value*	*Unit*
g	9.81	[m/s^2]
$m1$	7720	[kg]
$m2$	31300	[kg]
$I1$	$5.8733 \cdot 10^4$	[kgm^2]
$I2$	$1.1663 \cdot 10^6$	[kgm^2]
$x1$	1.9249	[m]
$x2$	5.0633	[m]
af	3.1	[m]
ar	0.6	[m]
as	7.68	[m]
bf	1.025	[m]
br	0.925	[m]
bs	1.0	[m]

Table 1 Vehicle parameters.

All scenarios are with free-rolling vehicles. In reality many of the effects that have been provoced by manipulating road-surface and tire parameters may be consequences of driving or braking differently on different axles.

The controllers were implemented in discrete-time with a sampling period of 50 ms.

6.1 Tractor Understeer — Uncontrolled

Scenario: Understeered single tractor vehicle in maneuver with sinusoidal steering angle with increasing amplitude.

Results: Reduced maneuverability with understeering at large steering amplitudes, due to saturated lateral adhesion forces on the front axle.

Simulation results are found in Appendix A.1.

6.2 Tractor Understeer — Controlled

Scenario: Understeered single tractor vehicle in maneuver with sinusoidal steering angle with increasing amplitude.

Controllers:

$$Q_f = \text{diag}\,[1,1] \qquad R_f = 10 \tag{68a}$$
$$Q_r = \text{diag}\,[10,3] \qquad R_r = 0.5 \tag{68b}$$

Results: Improved maneverability with braking interventions on front and rear axles. Overcompensation on the rear axle result in control interventions on the front axle.

Simulation results are found in Appendix A.2

6.3 Tractor Oversteer — Uncontrolled

Scenario: Oversteered single tractor vehicle in maneuver with sinusoidal steering angle with increasing amplitude.

Results: Spin-out due to saturating adhesion forces on the rear axle..

Simulation results are found in Appendix A.3.

6.4 Tractor Oversteer — Controlled

Scenario: Oversteered single tractor vehicle in maneuver with sinusoidal steering angle with increasing amplitude.

Controllers:

$$Q_f = \text{diag}\,[1,1] \qquad R_f = 10 \tag{69a}$$
$$Q_r = \text{diag}\,[10,3] \qquad R_r = 0.1 \tag{69b}$$

Results: Spin-out is prevented with control actions on the front axle.

Simulation results are found in Appendix A.4.

6.5 Tracor-Semitrailer Trailer-Swing — Uncontrolled

Scenario: Tractor-semitrailer vehicle in step-steering angle maneuver.

Results: Trailer-swing due to saturating adhesion forces on the semitrailer axle.

Simulation results are found in Appendix A.8.

6.6 Tracor-Semitrailer Trailer-Swing — Controlled Tractor

Scenario: Tractor-semitrailer vehicle in step-steering angle maneuver.

Controllers:

$$Q_f = \text{diag}\,[1,1] \qquad R_f = 10 \tag{70a}$$
$$Q_r = \text{diag}\,[10,3] \qquad R_r = 0.1 \tag{70b}$$

Results: Trailer-swing due to saturating adhesion forces on the semitrailer axle. The controller is designed for the tractor dynamics, and has no way to detect the swinging trailer.

Simulation results are found in Appendix A.9.

6.7 Tracor-Semitrailer Trailer-Swing — Controlled Tractor and Semitrailer

Scenario: Tractor-semitrailer vehicle in step-steering angle maneuver.

Controllers:

$$Q_f = \text{diag}\,[1,1,1,1] \qquad R_f = 1 \tag{71a}$$
$$Q_r = \text{diag}\,[1,1,10,10] \qquad R_r = 1 \tag{71b}$$
$$Q_s = \text{diag}\,[0,0,1,1] \qquad R_s = 10 \tag{71c}$$

Results: Trailer-swing prevented by control interventions on the rear axle. It is interesting to notice that semitrailer axle braking is not necessary to prevent the trailer-swing. The difference from the controller of Scenario A.9 is that a model of the semitrailer is included in the controller design.

Controllers tuning with more aggressive actuation on the semitrailer was also evaluated. They generally performed worse than the uncontrolled vehicle. This may be explained by the reduced stabilizing lateral adhesion force on the semitrailer axle during braking.

Simulation results are found in Appendix A.10.

6.8 Tracor-Semitrailer Understeer — Uncontrolled

Scenario: Understeered tractor-semitrailer vehicle in lane-change maneuver.

Results: Understeering due to saturating lateral adhesion forces on the front axle..

Simulation results are found in Appendix A.8.

6.9 Tracor-Semitrailer Understeer — Controlled Tractor

Scenario: Understeered tractor-semitrailer vehicle in lane-change maneuver.

Controllers:

$$Q_f = \text{diag}\,[1,1] \qquad R_f = 10 \tag{72a}$$
$$Q_r = \text{diag}\,[10,3] \qquad R_r = 0.1 \tag{72b}$$
$$\tag{72c}$$

Results: Improved tracking performance with control interventions on the rear axle.

Simulation results are found in Appendix A.9.

6.10 Tracor-Semitrailer Understeer — Controlled Tractor and Semitrailer

Scenario: Understeered tractor-semitrailer vehicle in lane-change maneuver.

Controllers:

$$Q_f = \text{diag}\,[1,1,0,0] \qquad R_f = 10 \tag{73a}$$
$$Q_r = \text{diag}\,[10,3,0,0] \qquad R_r = 0.1 \tag{73b}$$
$$Q_s = \text{diag}\,[0,0,1,1] \qquad R_s = 1 \tag{73c}$$

Results: Improved tracking performance with control interventions on the rear axle and the semitrailer axle. The results are slightly better than for the controlled tractor of Scenario A.9.

Simulation results are found in Appendix A.10.

6.11 Tracor-Semitrailer Jackknifing — Uncontrolled

Scenario: Oversteered tractor-semitrailer vehicle in lane-change maneuver.

Results: Jackknifing due to saturating lateral adhesion forces on the rear axle.

Simulation results are found in Appendix A.11.

6.12 Tracor-Semitrailer Jackknifing — Controlled Tractor

Scenario: Oversteered tractor-semitrailer vehicle in lane-change maneuver.

Controllers:

$$Q_f = \text{diag}\,[1,1] \qquad R_f = 10 \tag{74a}$$
$$Q_r = \text{diag}\,[10,3] \qquad R_r = 0.1 \tag{74b}$$
$$\tag{74c}$$

Results: Jackknifing prevented with control actions on the rear axle.

Simulation results are found in Appendix A.12.

6.13 Tracor-Semitrailer Jackknifing — Controlled Tractor and Semitrailer

Scenario: Oversteered tractor-semitrailer vehicle in lane-change maneuver.

Controllers:

$$Q_f = \text{diag}\,[1,1,0,0] \qquad R_f = 10 \tag{75a}$$
$$Q_r = \text{diag}\,[10,3,0,0] \qquad R_r = 0.1 \tag{75b}$$
$$Q_s = \text{diag}\,[0,0,1,1] \qquad R_s = 1 \tag{75c}$$

Results: Jackknifing prevented with control actions on the rear axle. Performance similar to the controlled tractor in Scenario A.12.

Simulation results are found in Appendix A.13.

7. Conclusions

The results of Section 6 indicate that yaw-control performance may be slightly improved by using semitrailer braking actuation. An interesting observation was that trailer-swing may be effectively prevented without semitrailer braking actuation if the articulation angle and the articulation velocity is used for feedback. Moderate semitrailer braking was applied in the understeering and jackknifing scenarios with controlled tractor and semitrailer. The control performance was slightly better than for the controlled tractor. It has not been investigated whether this performance improval is due to the actual braking of the semitrailer, or the fact that a model of the full vehicle combination is included in the design of the front and rear axles controllers.

The main conclusion is that measurement and feedback of the articulation angle may lead to singificantly better performance. The effect of semitrailer braking needs to be investigated further.

8. Future work

Further investigations on the effect of semitrailer braking on stabilization performance are necessary. The piecewise-affine formulation of the single vehicle dynamics in Section 4.5 could be used to analyze bounds on stabilizable regions in the state-space. Brake dynamics should be included in the yaw-controller design.

9. References

[ÅW97] K. J. Åström and B. Wittenmark. *Computer-Controlled Systems: Theory and Design*. Prentice Hall International, 3 edition, 1997.

[Ban99] R. T. Bannatayne. Electronic braking control developments. *Automotive Engineering International*, pages 125–127, Feb 1999.

[BB00] R. M. Brach and R. M. Brach. Modeling combined braking and steering tyre forces. Technical report, SAE Paper 2000-01-0357, 2000.

[CGS00] V. Claesson, M. Gäfvert, and M. Sanfridson. Proposal for a distributed computer control system in a heavy-duty truck. Technical Report No. 00-16, Department of Computer Engineering, Chalmers Univ. of Technology, 2000. DICOSMOS Report.

[DAR00] S. V. Drakunov, B. Ashrafi, and A. Rosiglioni. Yaw control algorithm via sliding mode control. In *Proc. of the American Control Conference*, pages 580–583, Chicago, Illinois, June 2000.

[Edl91] S. Edlund. Tyre models: Subreport –91. Technical report, Volvo Truck Corporation, 1991. (classified).

[GL01] M. Gäfvert and O. Lindgärde. A 9-dof tractor-semitrailer dynamic handling model for advanced chassis control studies. Technical Report ISRN LUTFD2/TFRT–7597–SE, Department of Automatic Control, Lund Institute of Technology, Sweden, 2001. DICOSMOS Report.

[GSC00] M. Gafvert, M. Sanfridsson, and V. Claesson. Truck model for yaw and roll dynamics control. Technical Report ISRN LUTFD2/TFRT–7588–SE, Department of Automatic Control, Lund Institute of Technology, 2000. DICOSMOS Report.

[Hac98] A. Hac. Evaluation of two concepts in vehicle stability enhancement systems. Technical Report 98ME031, Delphi Automotive Systems, 1998.

[HHJ+97] F. Hecker, S. Hummel, O. Jundt, K.-D. Leimback, I. Faye, and H. Schramm. Vehicle dynamics control for commercial vehicles. Technical report, SAE Paper 973284, 1997.

[HR98] D. D. Hoffman and M. D. Rizzo. Chevrolet c5 corvette vehicle dynamics control system. Technical report, SAE Paper 980233, 1998.

[IS95] Y. Ikushima and K. Sawese. A study on the effects of the active yaw moment control. Technical report, SAE Paper 950303, 1995.

[Joh99] M. Johansson. *Piecewise Linear Control Systems*. PhD thesis, Department of Automatic Control, Lund Institiute of Technology, 1999.

[MSH+99] K. Matsuda, H. Shinjyo, M. Harada, K. Ohata, and K. Sakata. A study on heavy duty truck stability control by braking force control. *JSAE Review*, pages 87–91, 1999.

[PA99] J. H. Park and W. S. Ahn. h_∞ yaw-moment control with brakes for improving driving performance and stability. In *Proc. of the 1999 IEEE/ASME Internat. Conf. on Advanced Intelligent Mechatronics*, pages 747–752, Atlanta, USA, Sep 1999.

[PEG95] L. Palkovics and M. El-Gindy. Design of an active unilateral brake control system for five-axle tractor-semitrailer based on sensitivity analysis. *Vehicle Systems Dynamics*, 24:725–758, 1995.

[PF01] L. Palcovics and A. Fries. Intelligent electronic systems in commercial vehicles for enhanced traffic safety. *Vehicle Systems Dynamics*, 35(4–5):227–289, 2001.

[PNG+98] E. Petersen, D. Neuhaus, K. Gläbe, R. Koschorek, and T. Reich. Vehicle stability control for trucks and buses. Technical report, SAE Paper 982782, 1998.

[SCG00] M. Sanfridson, V. Claesson, and M. Gäfvert. Investigation and requirements of a computer control system in a heavy-duty truck. Technical Report TRITA-MMK 2000:5, ISSN 1400-1179, ISRN KTH/MMK–00/5–SE, Mechatronics Lab, Department of Machine Design, Royal Institute of Technology, 2000. DICOSMOS Report.

[SPP96] D. J. Schuring, W. Pelz, and M. G. Pottinger. A model for combined tire cornering and braking forces. Technical report, SAE Paper 960180, 1996.

[SST93] Y. Shibahata, K. Shimada, and T.Tomari. Improvement of vehicle maneuverability by direct yaw moment control. *Vehicle Systems Dynamics*, 22:465–481, 1993.

[vZ00] A.T. van Zanten. Bosch ESP systems: 5 years of experience. Technical report, SAE Paper 2000-01-1633, 2000.

[vZELP98] A. T. van Zanten, R. Erhard, Klaus Landesfeind, and G. Pfaff. VDC systems development and perspective. Technical report, SAE Paper 980235, 1998.

[vZEP95] A. T. van Zanten, R. Erhart, and G. Pfaff. VDC, the vehicle dynamics control system of bosch. Technical report, SAE Paper 950759, 1995.

[YAB+99] T. Yoshioka, T. Adachi, T. Butsuen, H. Okazaki, and H. Mochizuki. Application of sliding-mode theory to direct yaw-moment control. *JSAE Review*, 20:523–529, 1999.

A. Simulations

A.1 Tractor Understeer — Uncontrolled

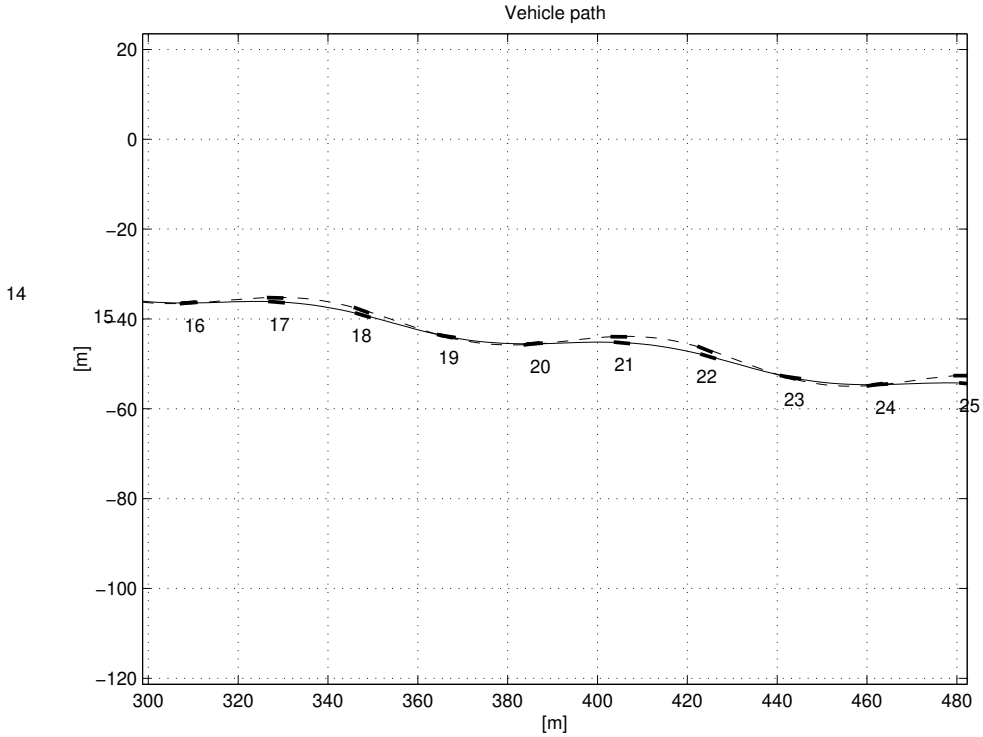

Figure 15 Vehicle trace

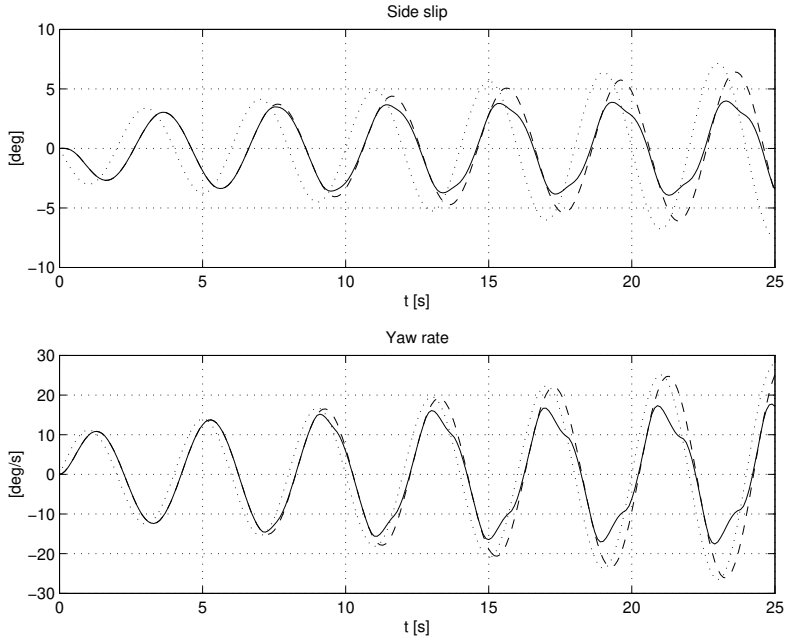

Figure 16 Vehicle states. (Solid: nonlinear model, Dashed: linear model, Dotted: steady-state)

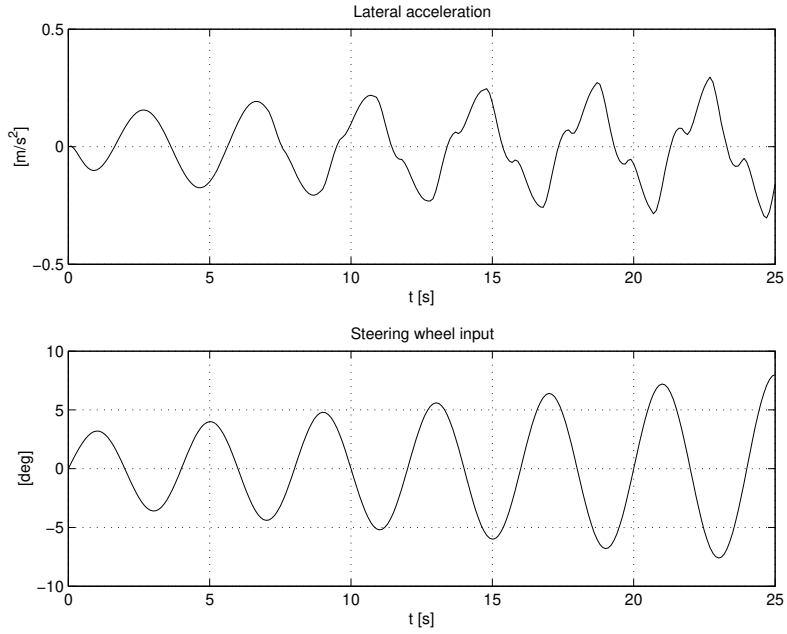

Figure 17 Lateral acceleration and steering input.

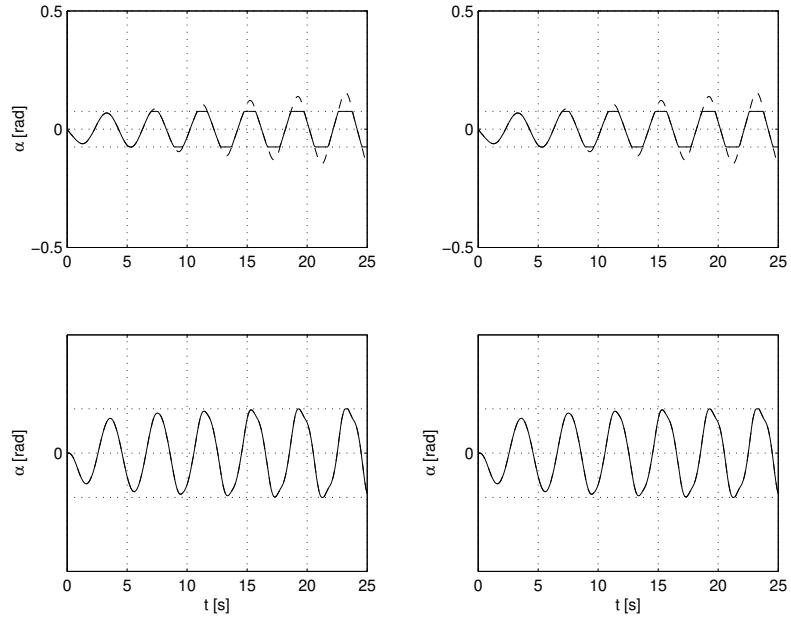

Figure 18 Side slips. (Solid: effective slip α', Dashed: actual slip α, Dotted: slip saturation limit α^*, Upper left: front left wheel, Upper right: front right wheel, Lower left: rear left wheel, Lower right: rear right wheel)

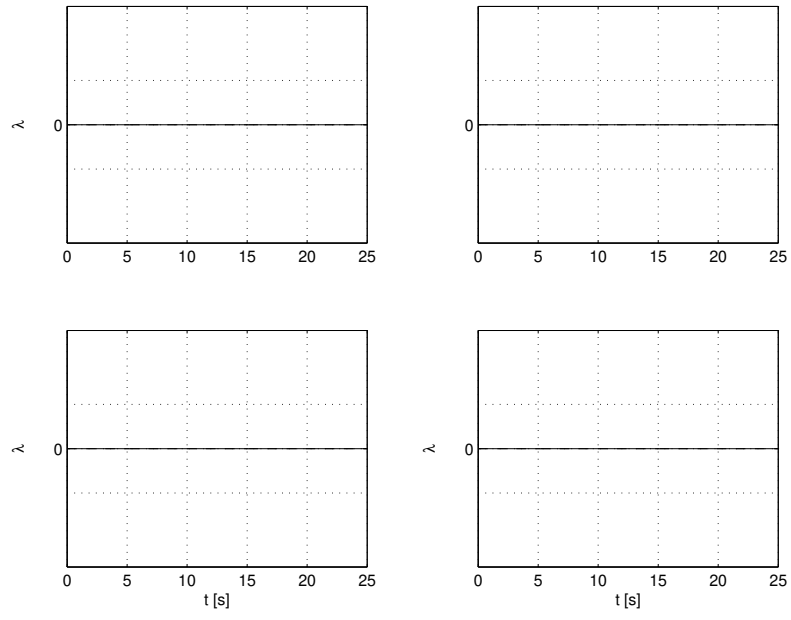

Figure 19 Longitudinal slips. (Solid: effective slip λ', Dashed: actual slip λ, Dotted: slip saturation limit λ^*, Upper left: front left wheel, Upper right: front right wheel, Lower left: rear left wheel, Lower right: rear right wheel)

A.2 Tractor Understeer — Controlled

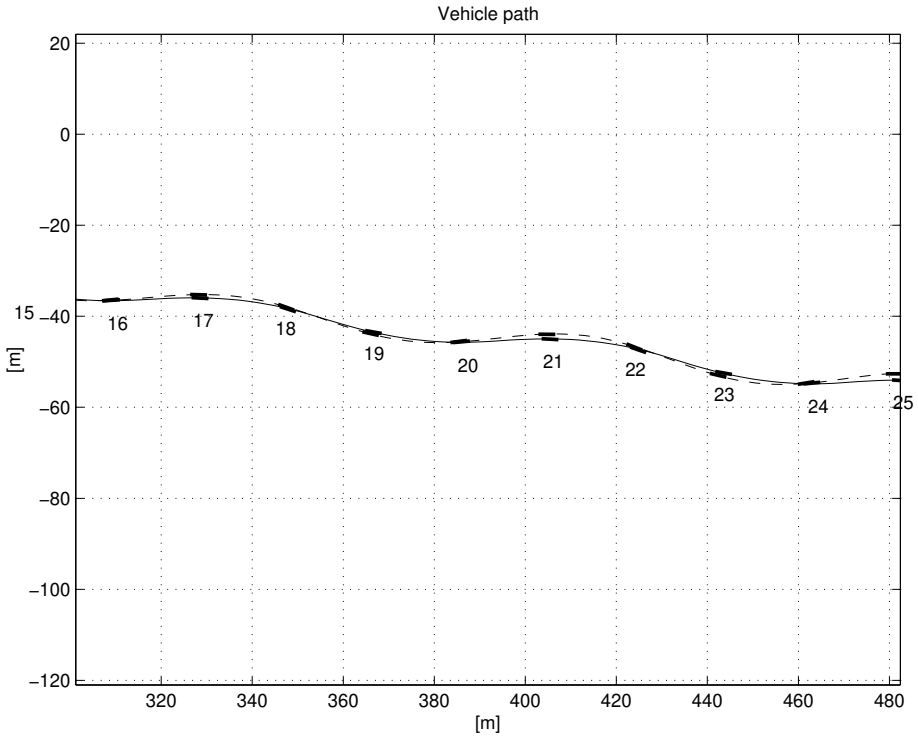

Figure 20 Vehicle trace

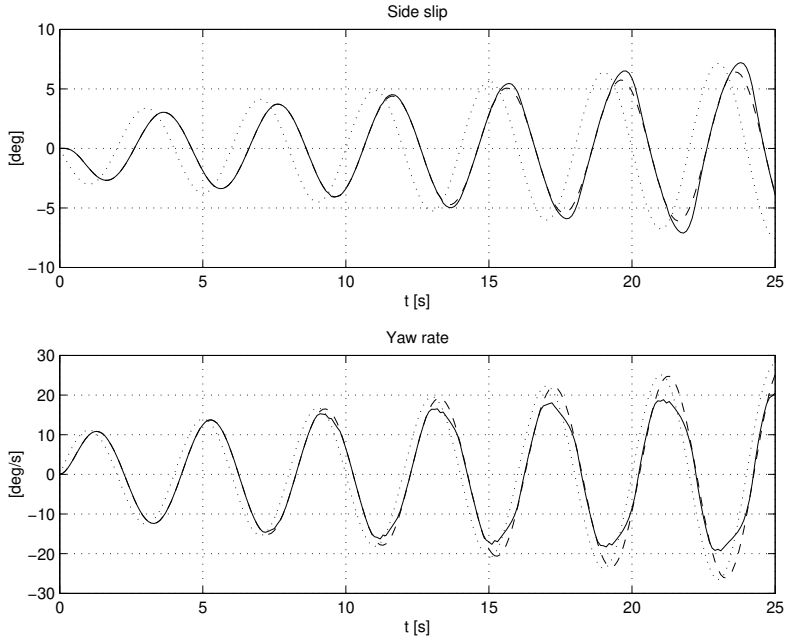

Figure 21 Vehicle states. (Solid: nonlinear model, Dashed: linear model, Dotted: steady-state)

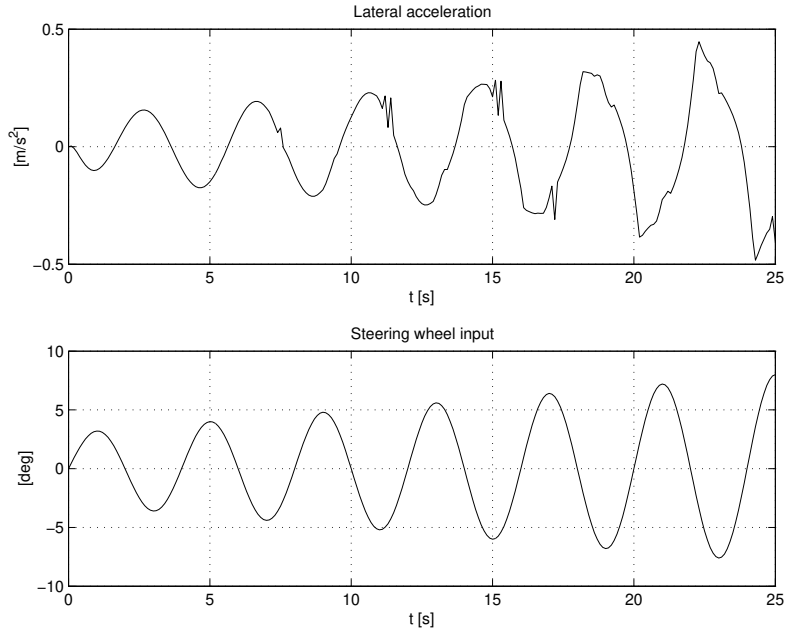

Figure 22 Lateral acceleration and steering input.

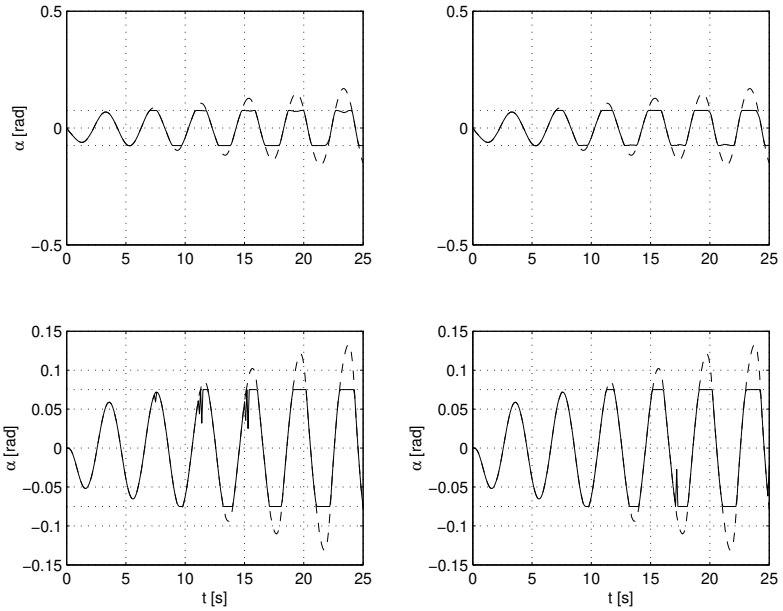

Figure 23 Side slips. (Solid: effective slip α', Dashed: actual slip α, Dotted: slip saturation limit α^*, Upper left: front left wheel, Upper right: front right wheel, Lower left: rear left wheel, Lower right: rear right wheel)

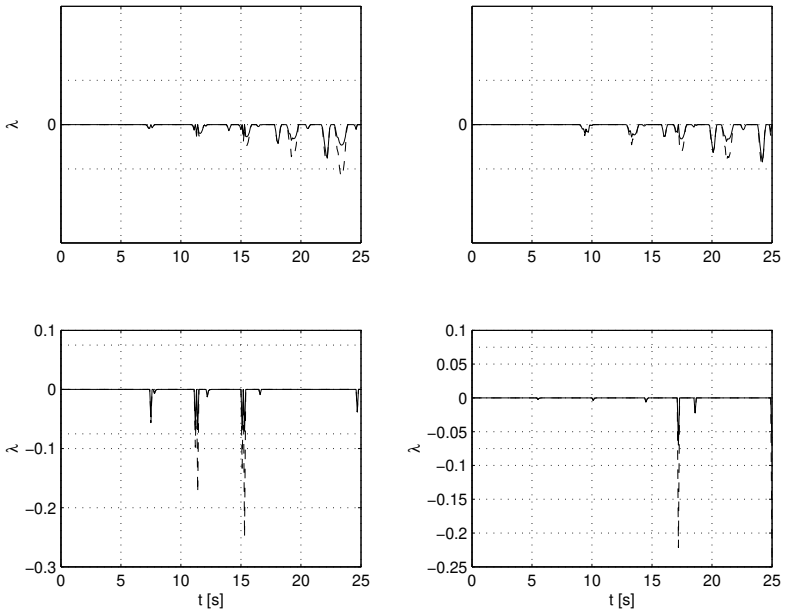

Figure 24 Longitudinal slips. (Solid: effective slip λ', Dashed: actual slip λ, Dotted: slip saturation limit λ^*, Upper left: front left wheel, Upper right: front right wheel, Lower left: rear left wheel, Lower right: rear right wheel)

A.3 Tractor Oversteer — Uncontrolled

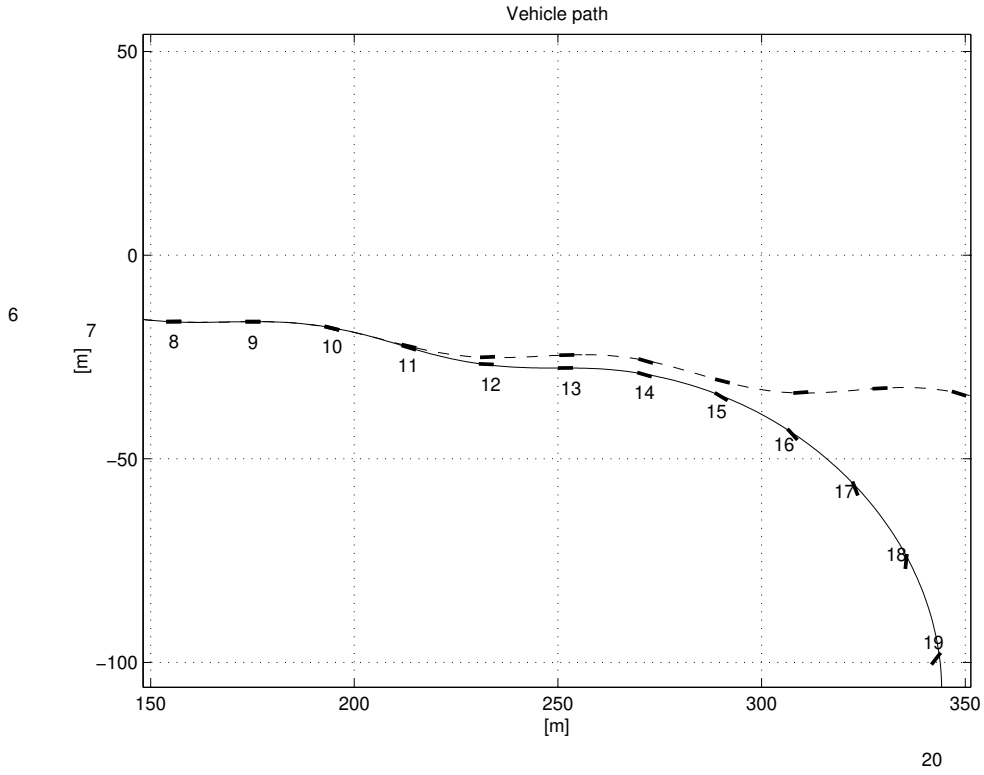

Figure 25 Vehicle trace for the linear reference model (dashed), and the controlled model with nonlinear tires.

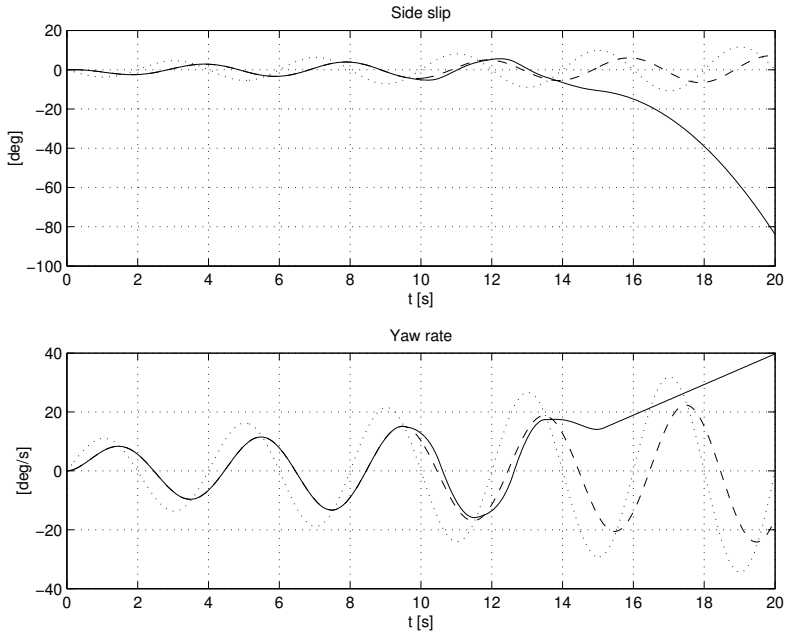

Figure 26 Vehicle states. (Solid: nonlinear model, Dashed: linear model, Dotted: steady-state)

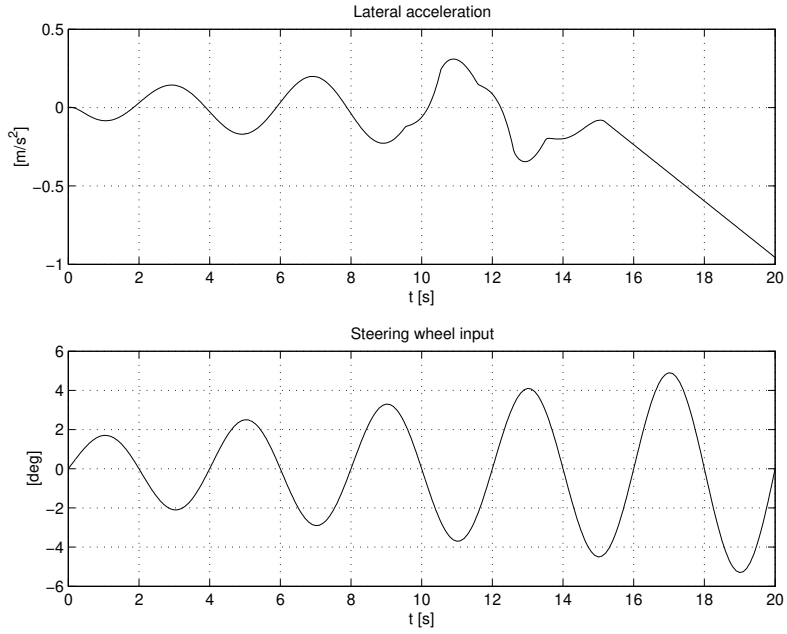

Figure 27 Lateral acceleration and steering input.

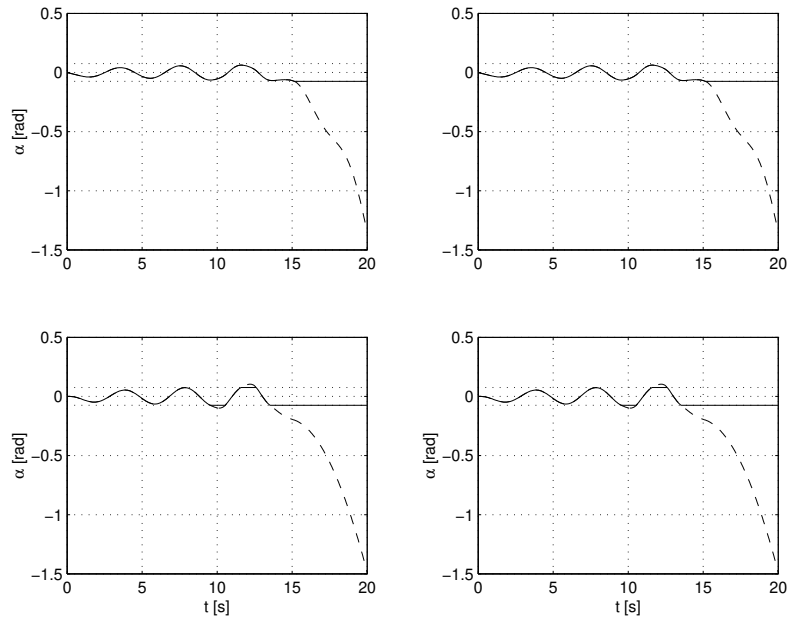

Figure 28 Side slips. (Solid: effective slip α', Dashed: actual slip α, Dotted: slip saturation limit α^*, Upper left: front left wheel, Upper right: front right wheel, Lower left: rear left wheel, Lower right: rear right wheel)

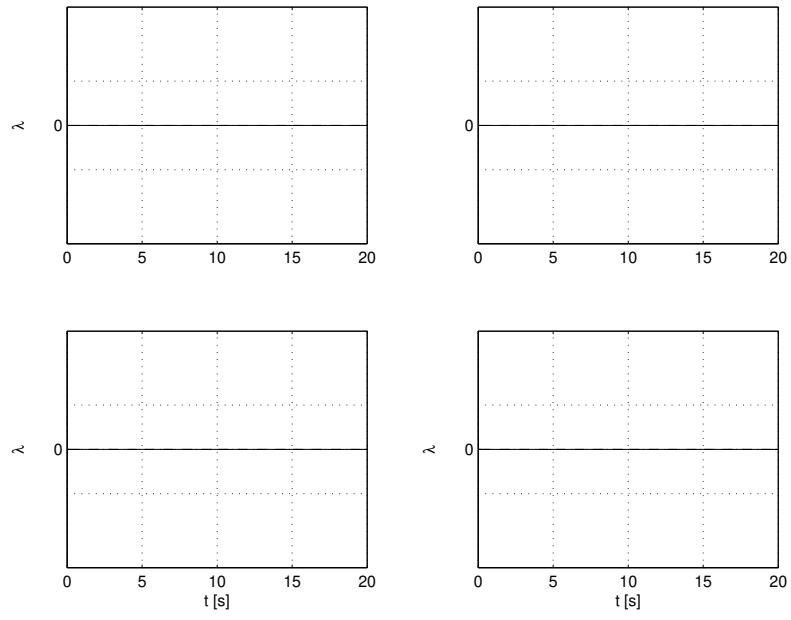

Figure 29 Longitudinal slips. (Solid: effective slip λ', Dashed: actual slip λ, Dotted: slip saturation limit λ^*, Upper left: front left wheel, Upper right: front right wheel, Lower left: rear left wheel, Lower right: rear right wheel)

A.4 Tractor Oversteer — Controlled

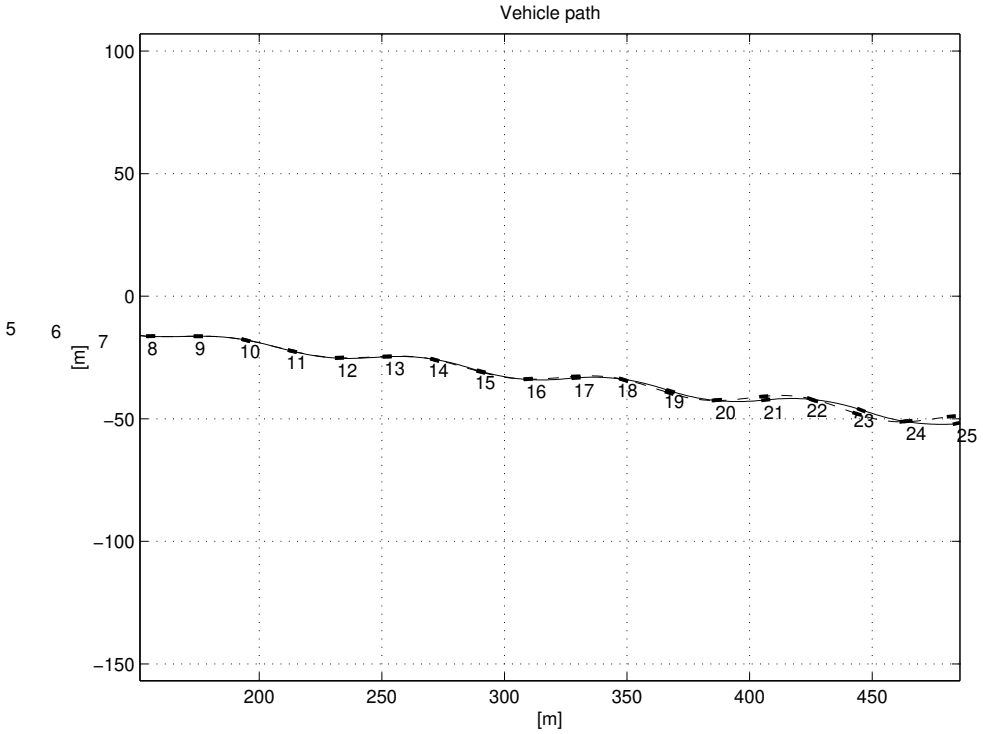

Figure 30 Vehicle trace for the linear reference model (dashed), and the controlled model with nonlinear tires.

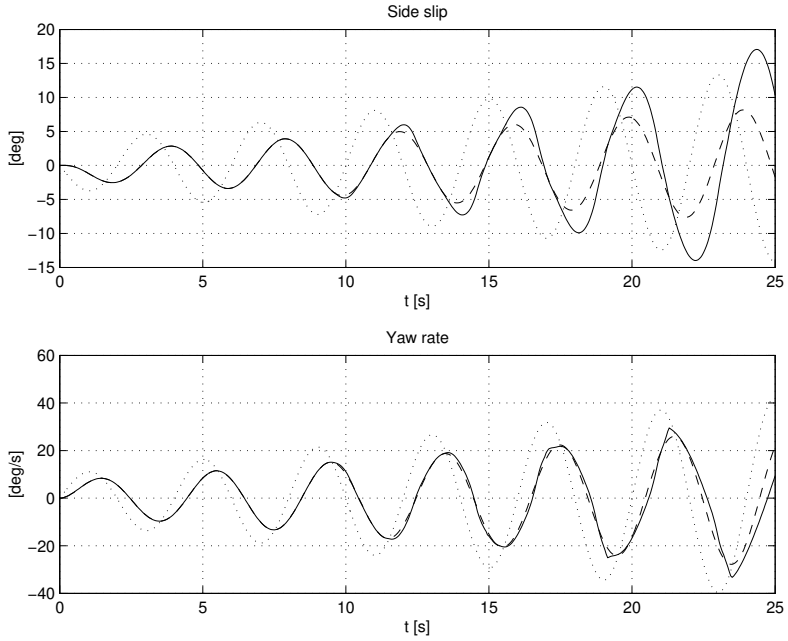

Figure 31 Vehicle states. (Solid: nonlinear model, Dashed: linear model, Dotted: steady-state)

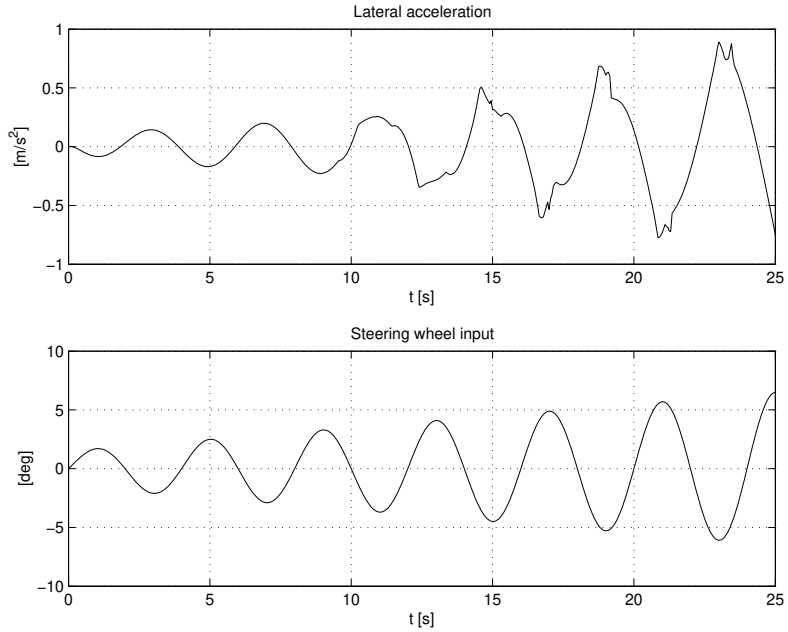

Figure 32 Lateral acceleration and steering input.

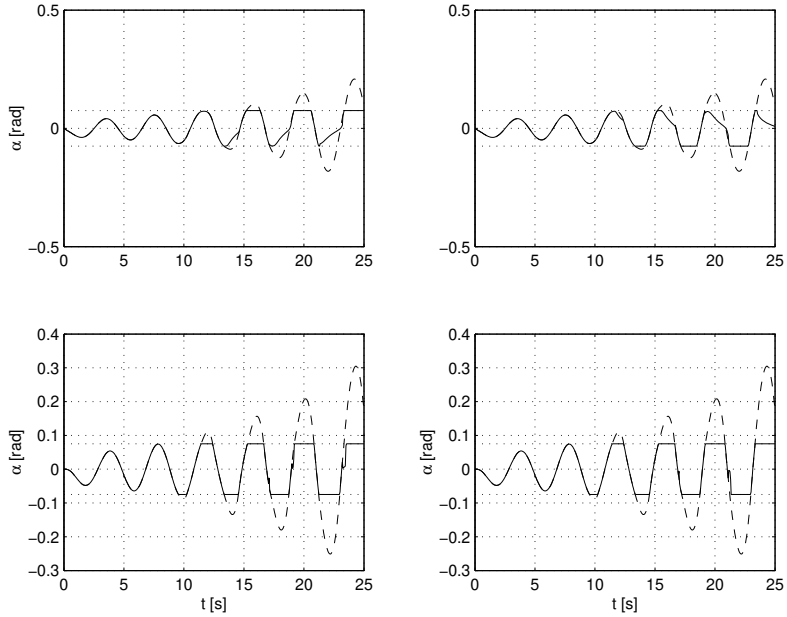

Figure 33 Side slips. (Solid: effective slip α', Dashed: actual slip α, Dotted: slip saturation limit α^*, Upper left: front left wheel, Upper right: front right wheel, Lower left: rear left wheel, Lower right: rear right wheel)

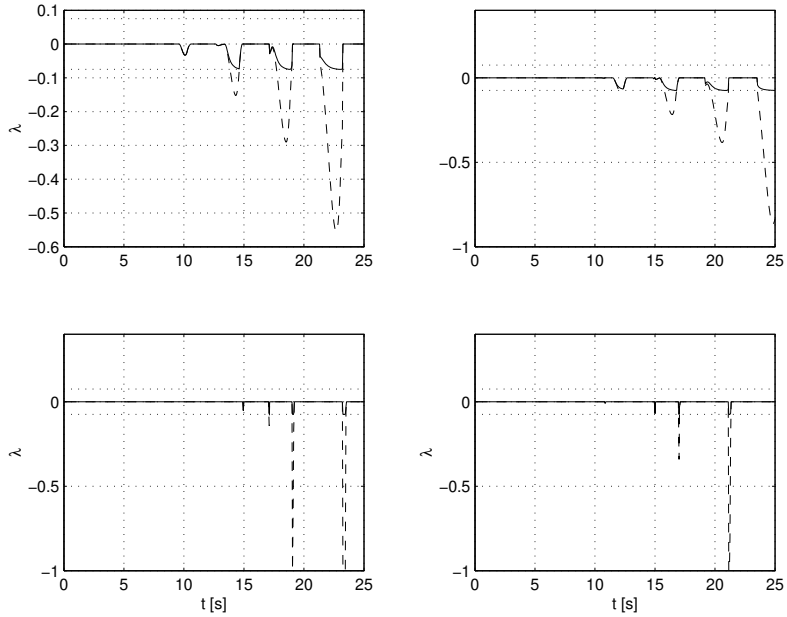

Figure 34 Longitudinal slips. (Solid: effective slip λ', Dashed: actual slip λ, Dotted: slip saturation limit λ^*, Upper left: front left wheel, Upper right: front right wheel, Lower left: rear left wheel, Lower right: rear right wheel)

A.5 Tractor-Semitrailer Trailer-Swing — Uncontrolled

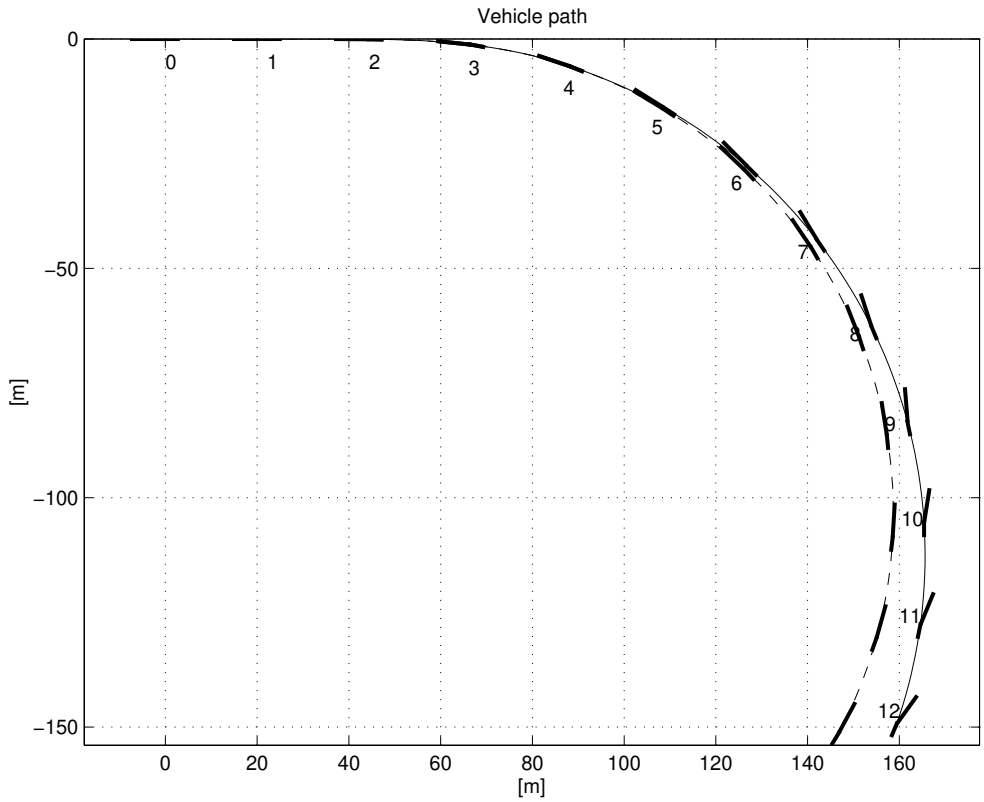

Figure 35 Vehicle trace for the linear reference model (dashed), and the controlled model with nonlinear tires.

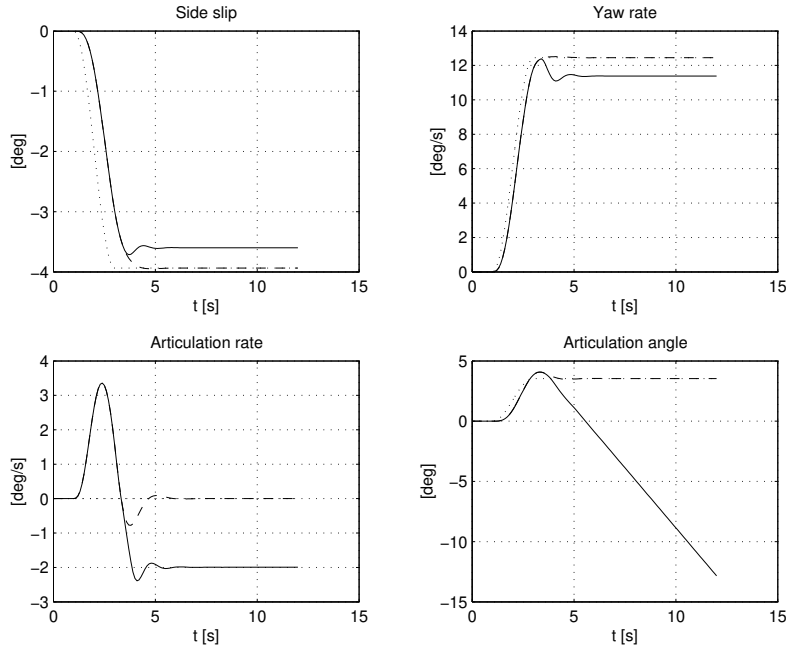

Figure 36 Vehicle states. (Solid: nonlinear model, Dashed: linear model, Dotted: steady-state)

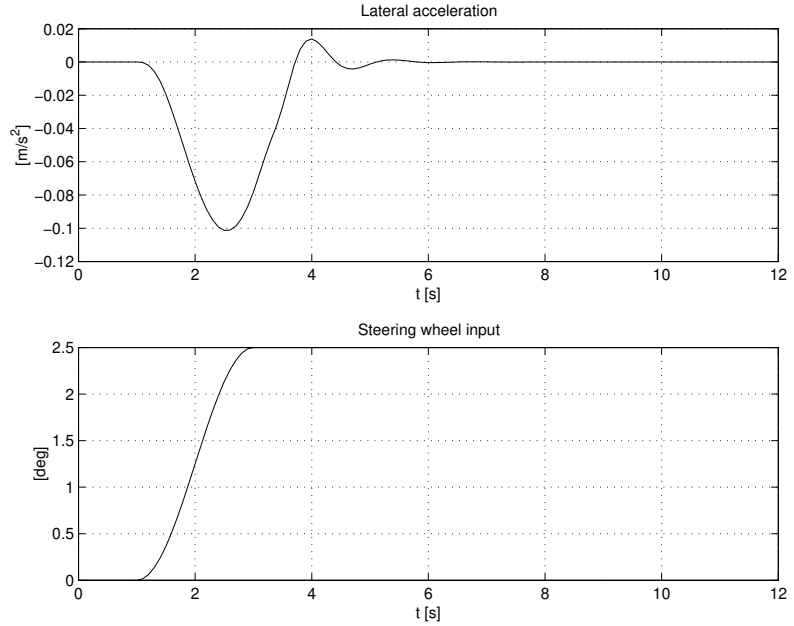

Figure 37 Lateral acceleration and steering input.

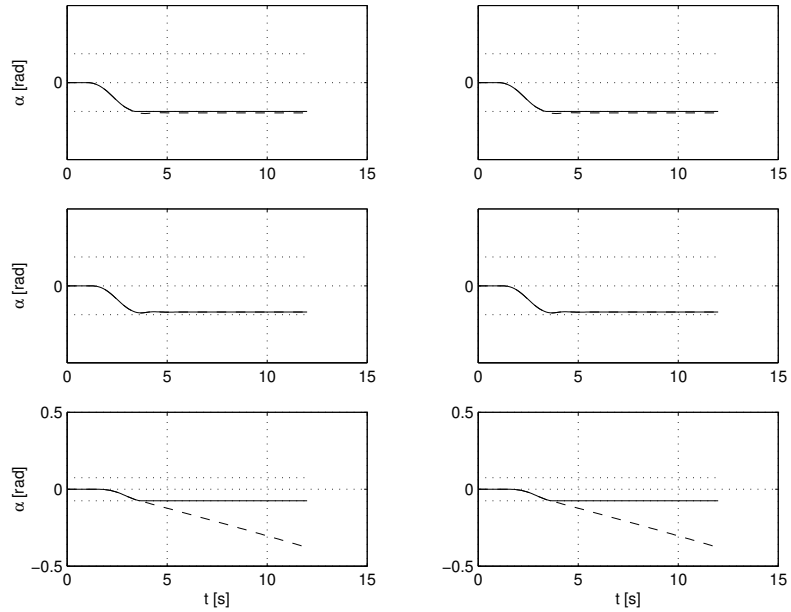

Figure 38 Side slips. (Solid: effective slip α', Dashed: actual slip α, Dotted: slip saturation limit α^*, Upper left: front left wheel, Upper right: front right wheel, Middle left: rear left wheel, Middle right: rear right wheel, Lower left: semitrailer left wheel, Lower right: semitrailer right wheel)

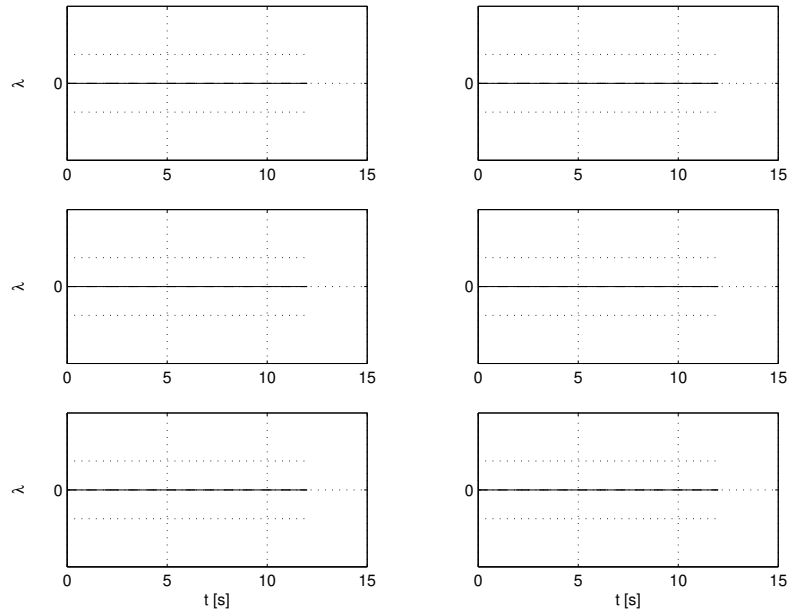

Figure 39 Longitudinal slips. (Solid: effective slip λ', Dashed: actual slip λ, Dotted: slip saturation limit λ^*, Upper left: front left wheel, Upper right: front right wheel, Middle left: rear left wheel, Middle right: rear right wheel, Lower left: semitrailer left wheel, Lower right: semitrailer right wheel)

A.6 Tractor-Semitrailer Trailer-Swing — Controlled Tractor

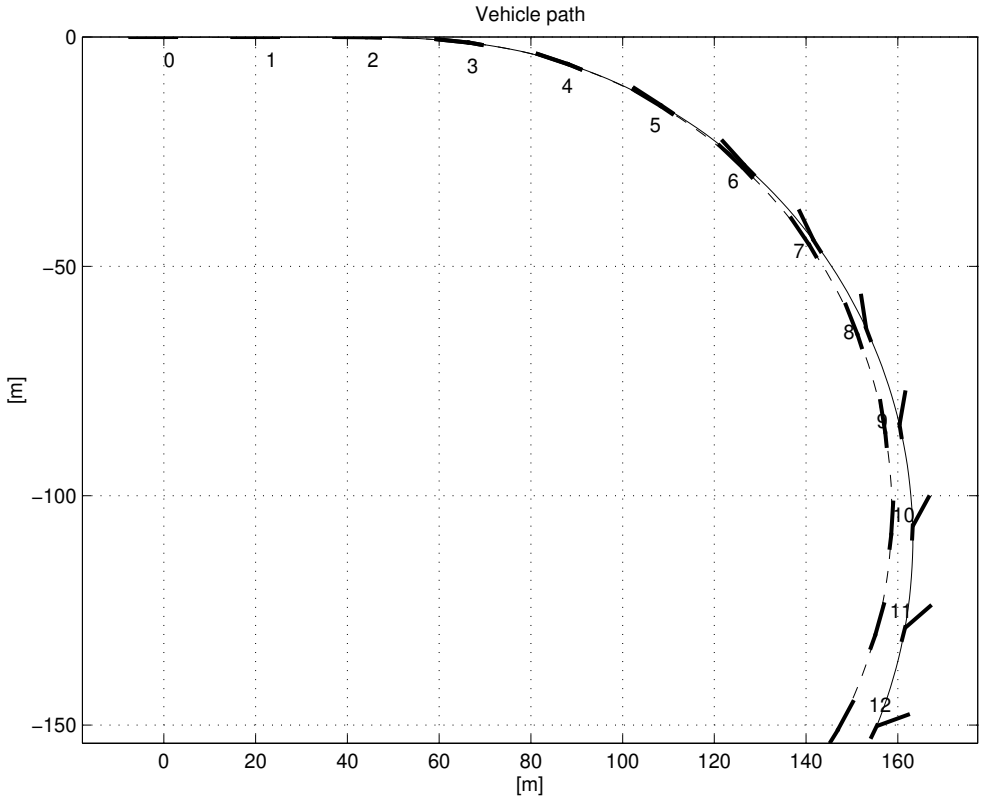

Figure 40 Vehicle trace for the linear reference model (dashed), and the controlled model with nonlinear tires.

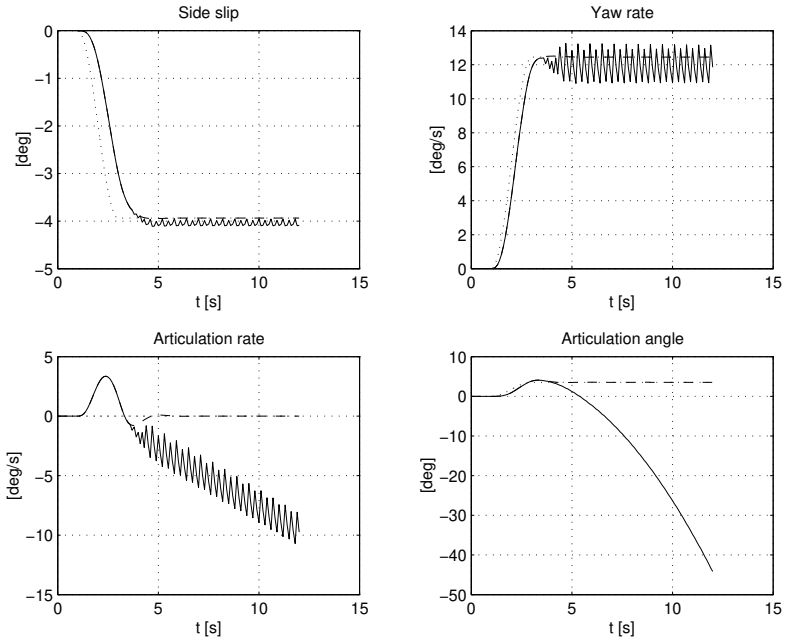

Figure 41 Vehicle states. (Solid: nonlinear model, Dashed: linear model, Dotted: steady-state)

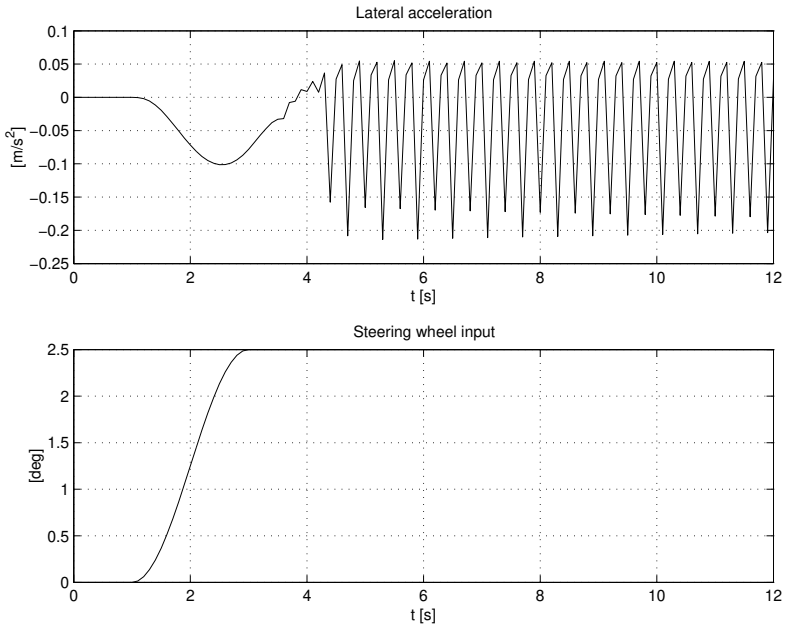

Figure 42 Lateral acceleration and steering input.

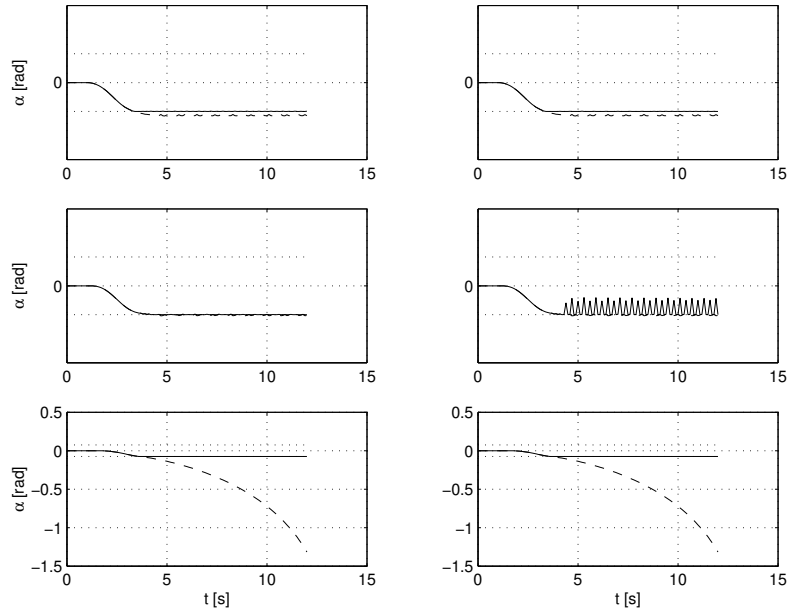

Figure 43 Side slips. (Solid: effective slip α', Dashed: actual slip α, Dotted: slip saturation limit α^*, Upper left: front left wheel, Upper right: front right wheel, Middle left: rear left wheel, Middle right: rear right wheel, Lower left: semitrailer left wheel, Lower right: semitrailer right wheel)

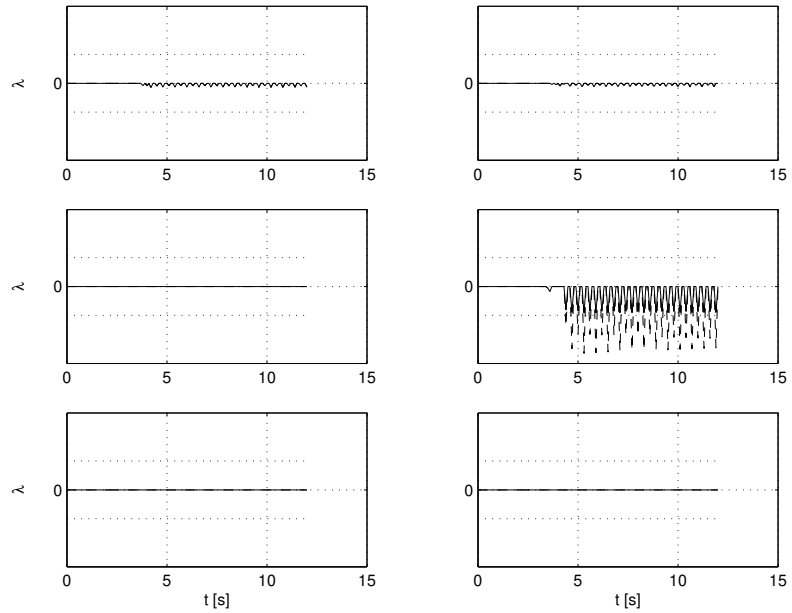

Figure 44 Longitudinal slips. (Solid: effective slip λ', Dashed: actual slip λ, Dotted: slip saturation limit λ^*, Upper left: front left wheel, Upper right: front right wheel, Middle left: rear left wheel, Middle right: rear right wheel, Lower left: semitrailer left wheel, Lower right: semitrailer right wheel)

A.7 Tractor-Semitrailer Trailer-Swing — Controlled Tractor and Semi-Trailer

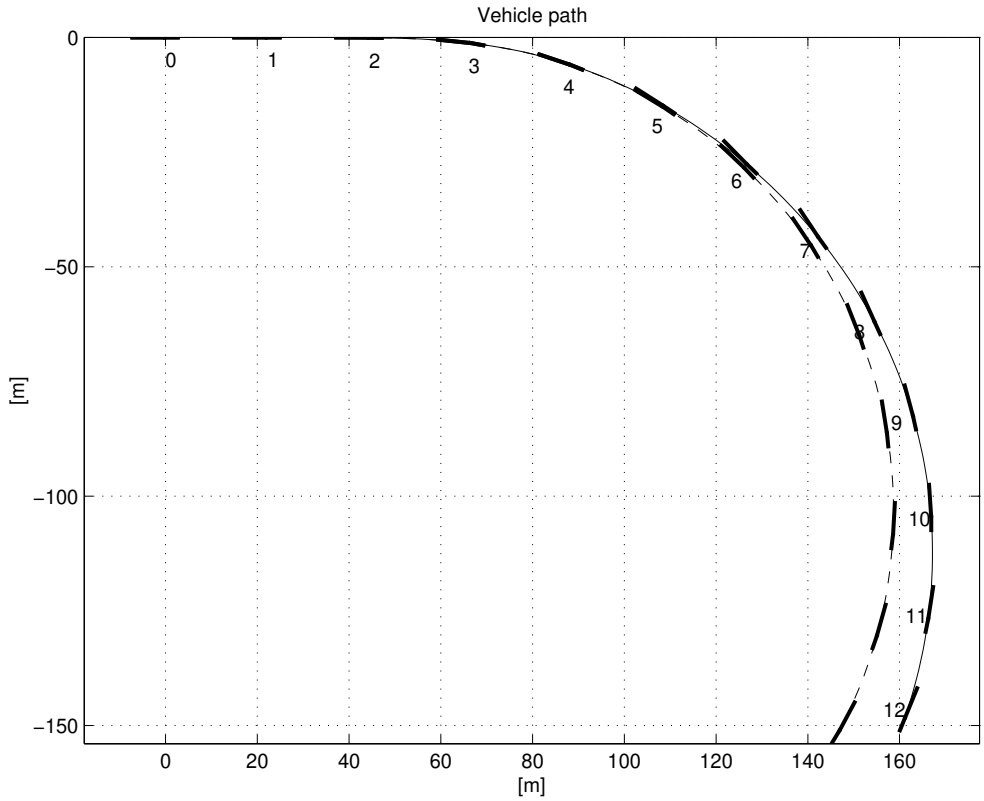

Figure 45 Vehicle trace for the linear reference model (dashed), and the controlled model with nonlinear tires.

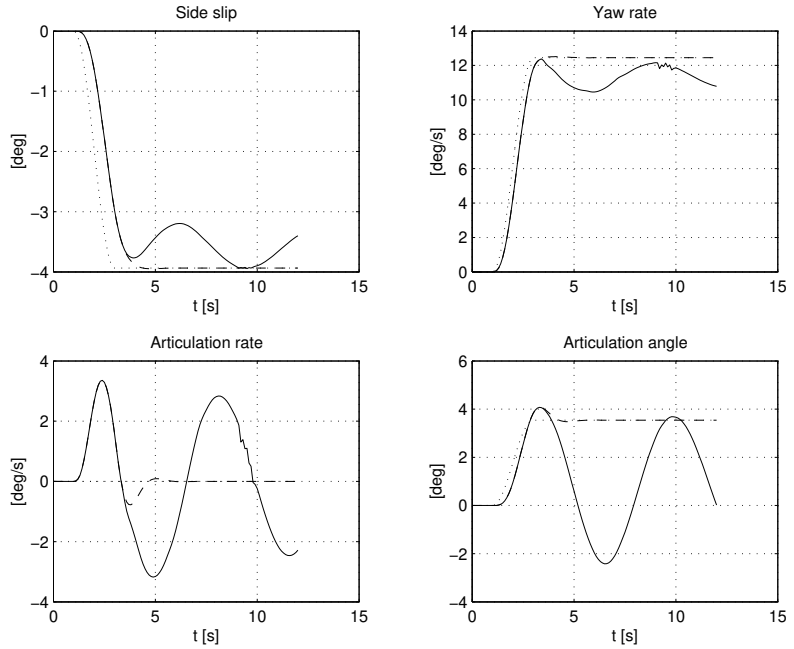

Figure 46 Vehicle states. (Solid: nonlinear model, Dashed: linear model, Dotted: steady-state)

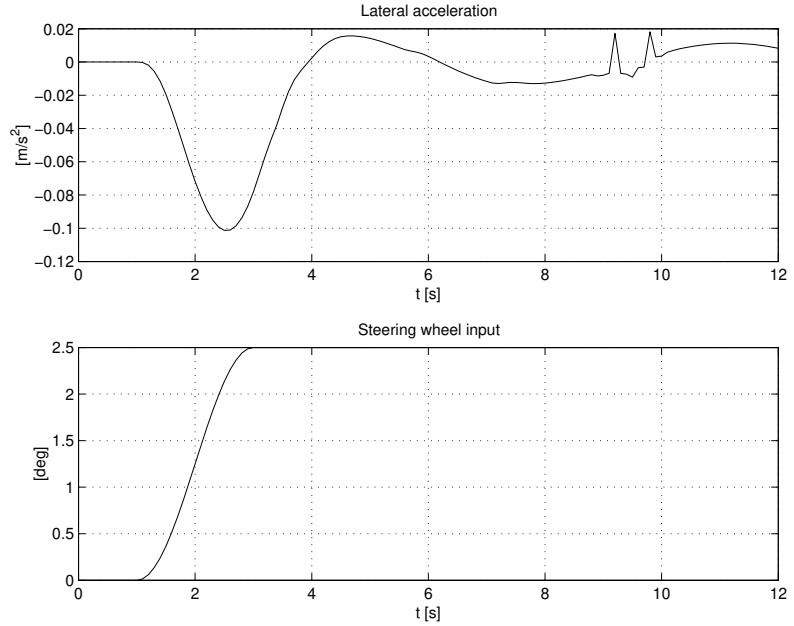

Figure 47 Lateral acceleration and steering input.

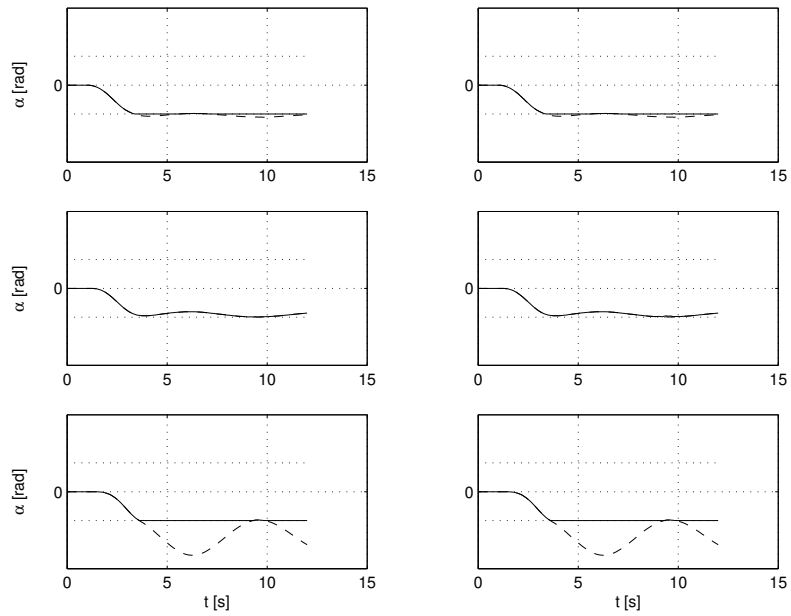

Figure 48 Side slips. (Solid: effective slip α', Dashed: actual slip α, Dotted: slip saturation limit α^*, Upper left: front left wheel, Upper right: front right wheel, Middle left: rear left wheel, Middle right: rear right wheel, Lower left: semitrailer left wheel, Lower right: semitrailer right wheel)

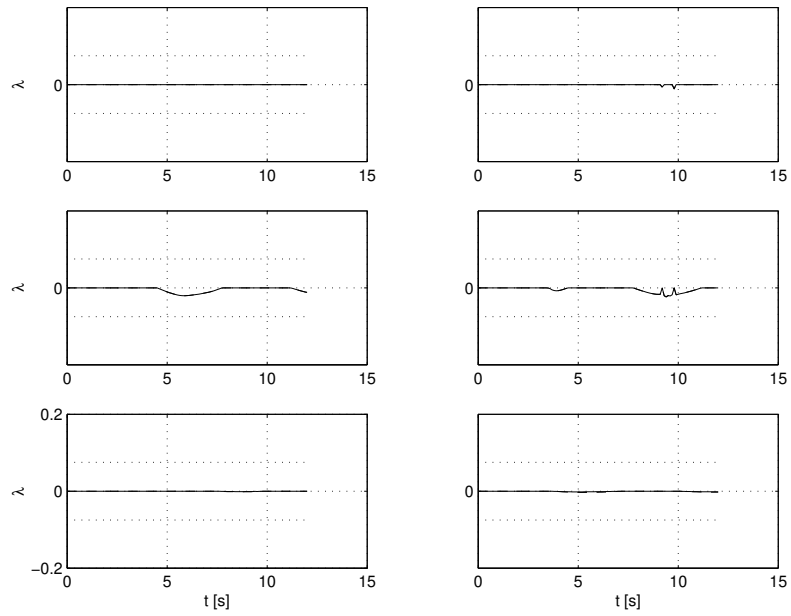

Figure 49 Longitudinal slips. (Solid: effective slip λ', Dashed: actual slip λ, Dotted: slip saturation limit λ^*, Upper left: front left wheel, Upper right: front right wheel, Middle left: rear left wheel, Middle right: rear right wheel, Lower left: semitrailer left wheel, Lower right: semitrailer right wheel)

A.8 Tractor-Semitrailer Understeer — Uncontrolled

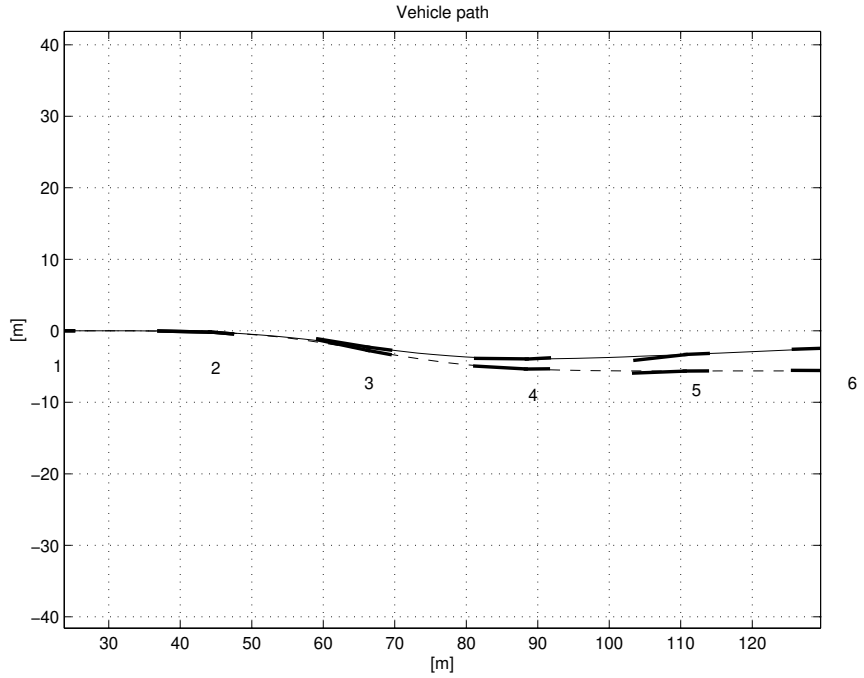

Figure 50 Vehicle trace for the linear reference model (dashed), and the controlled model with nonlinear tires.

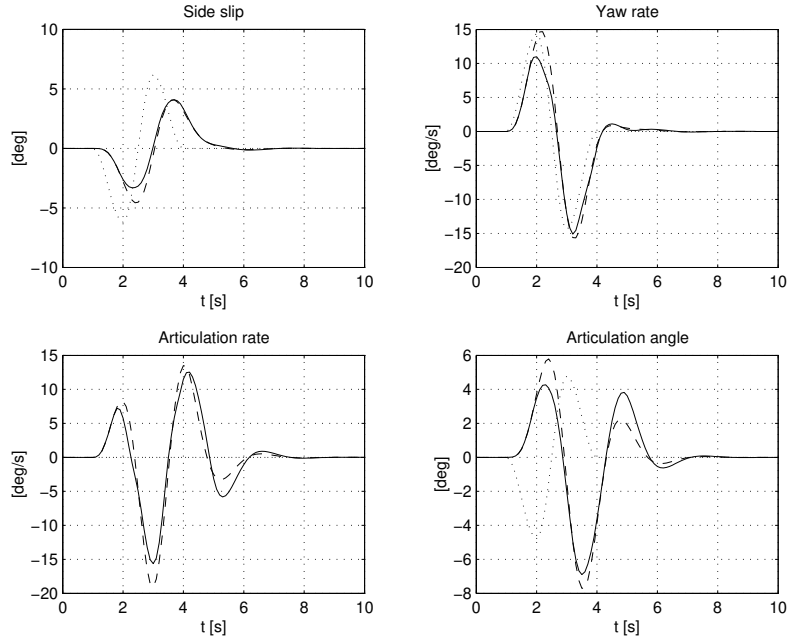

Figure 51 Vehicle states. (Solid: nonlinear model, Dashed: linear model, Dotted: steady-state)

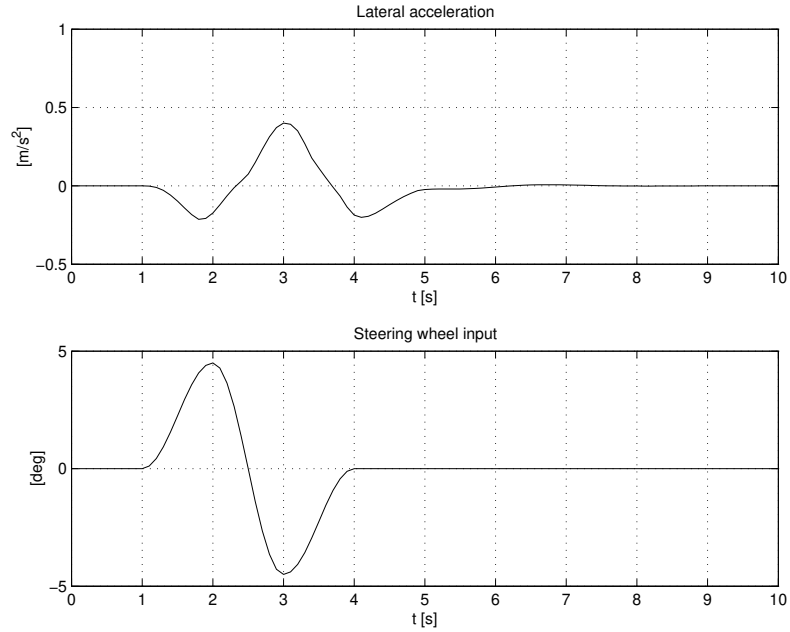

Figure 52 Lateral acceleration and steering input.

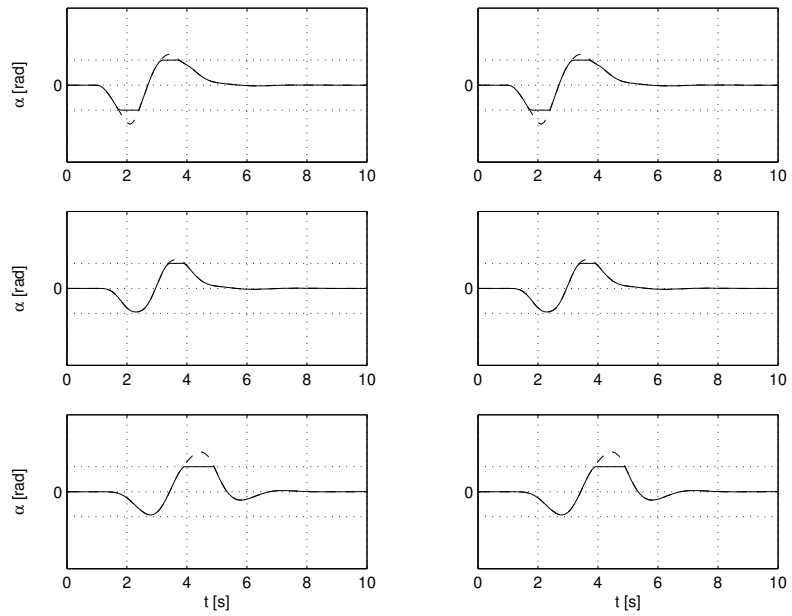

Figure 53 Side slips. (Solid: effective slip α', Dashed: actual slip α, Dotted: slip saturation limit α^*, Upper left: front left wheel, Upper right: front right wheel, Middle left: rear left wheel, Middle right: rear right wheel, Lower left: semitrailer left wheel, Lower right: semitrailer right wheel)

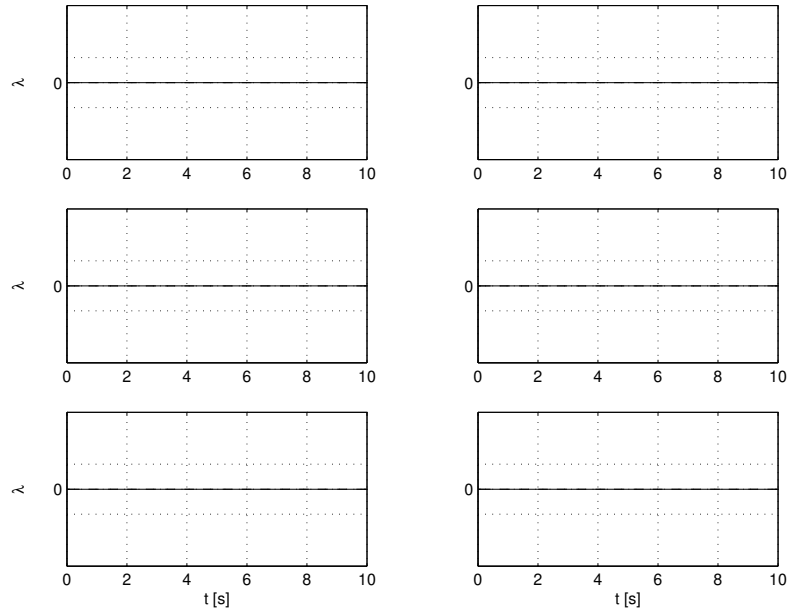

Figure 54 Longitudinal slips. (Solid: effective slip λ', Dashed: actual slip λ, Dotted: slip saturation limit λ^*, Upper left: front left wheel, Upper right: front right wheel, Middle left: rear left wheel, Middle right: rear right wheel, Lower left: semitrailer left wheel, Lower right: semitrailer right wheel)

A.9 Tractor-Semitrailer Understeer — Controlled Tractor

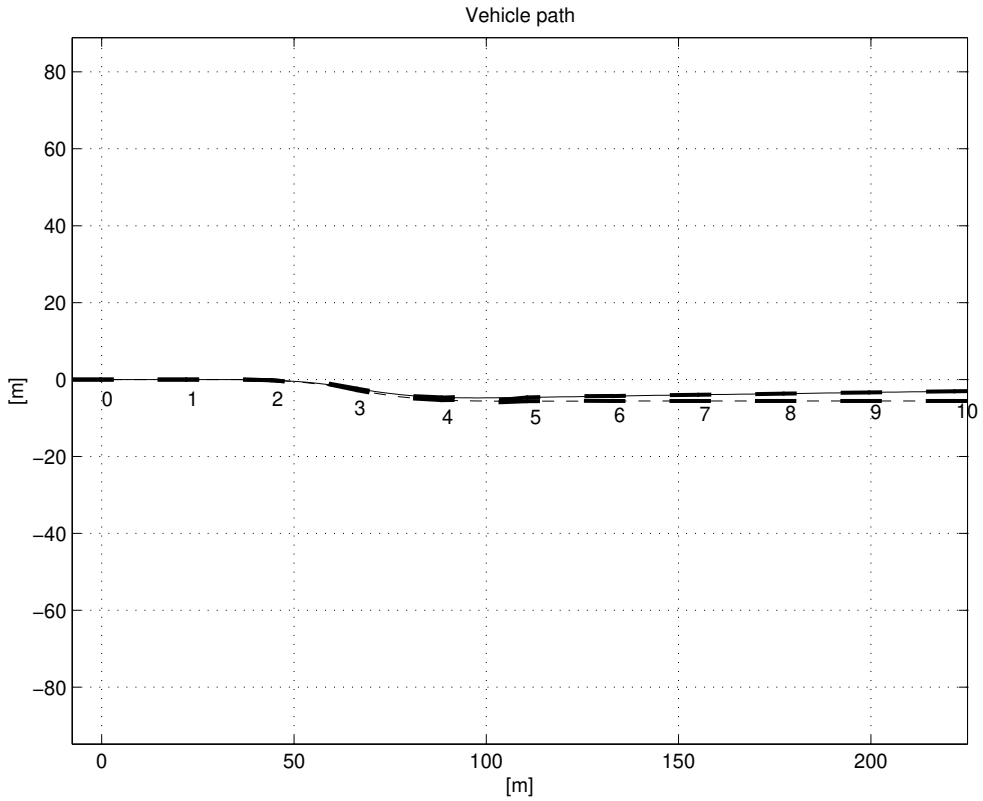

Figure 55 Vehicle trace for the linear reference model (dashed), and the controlled model with nonlinear tires.

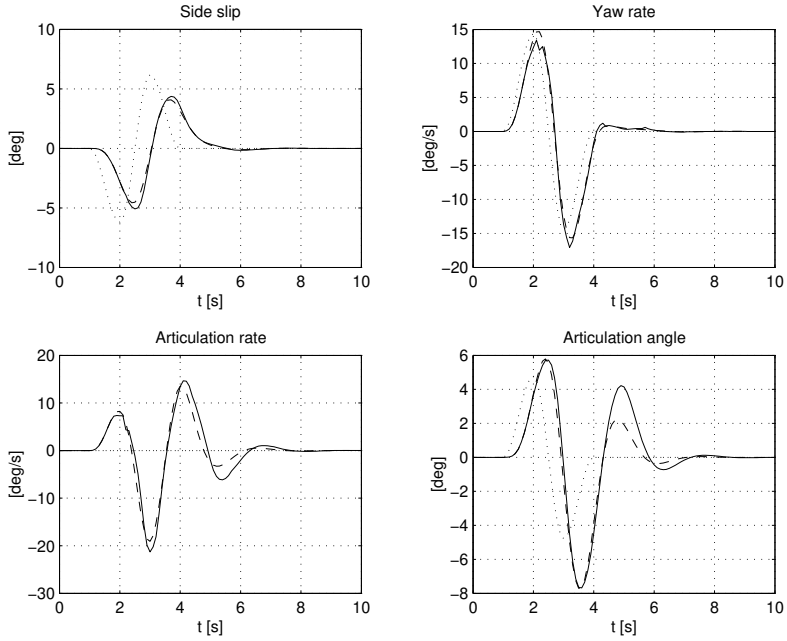

Figure 56 Vehicle states. (Solid: nonlinear model, Dashed: linear model, Dotted: steady-state)

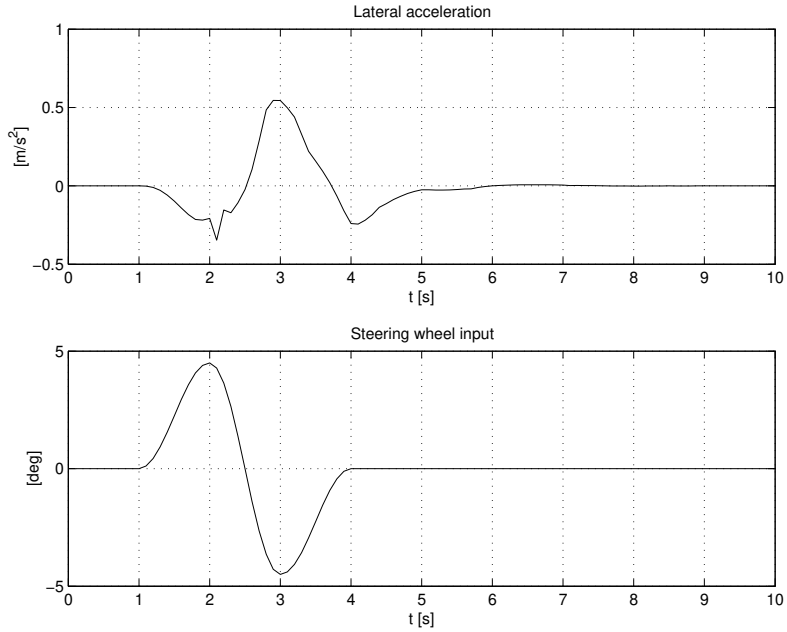

Figure 57 Lateral acceleration and steering input.

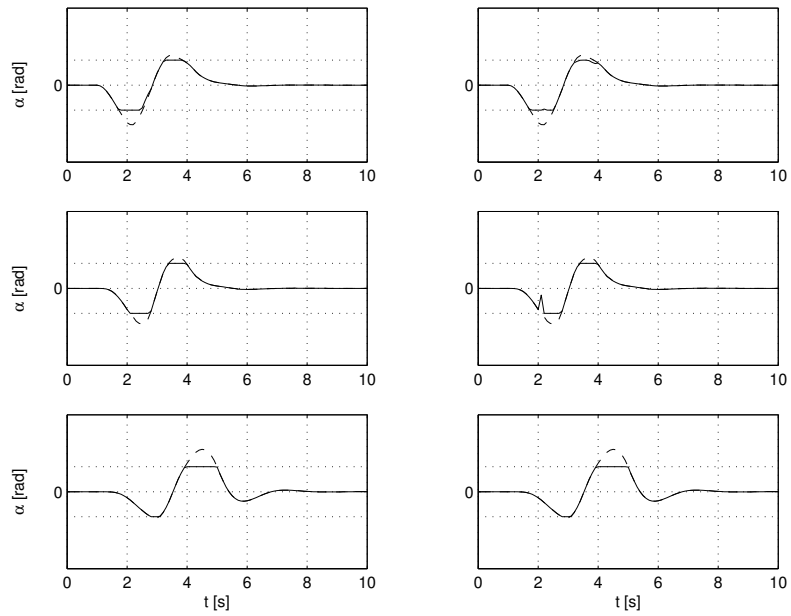

Figure 58 Side slips. (Solid: effective slip α', Dashed: actual slip α, Dotted: slip saturation limit α^*, Upper left: front left wheel, Upper right: front right wheel, Middle left: rear left wheel, Middle right: rear right wheel, Lower left: semitrailer left wheel, Lower right: semitrailer right wheel)

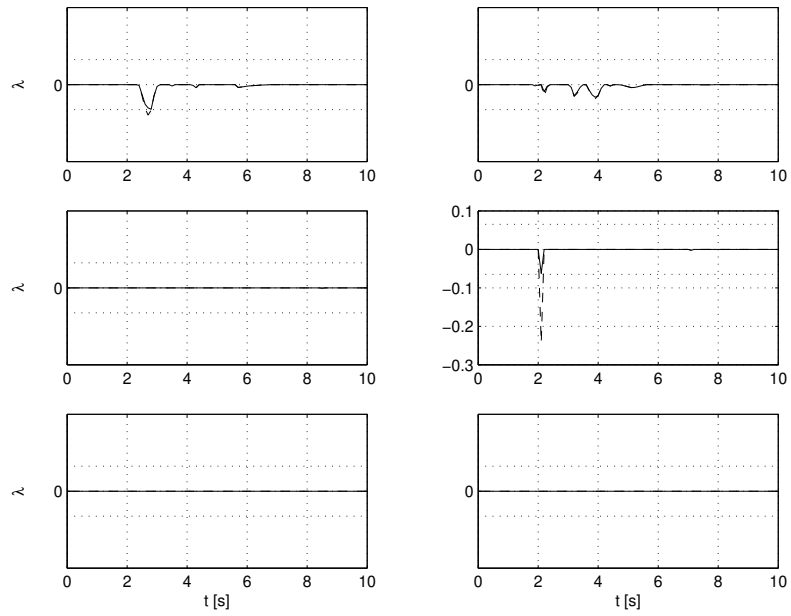

Figure 59 Longitudinal slips. (Solid: effective slip λ', Dashed: actual slip λ, Dotted: slip saturation limit λ^*, Upper left: front left wheel, Upper right: front right wheel, Middle left: rear left wheel, Middle right: rear right wheel, Lower left: semitrailer left wheel, Lower right: semitrailer right wheel)

A.10 Tractor-Semitrailer Understeer — Controlled Tractor and Semi-Trailer

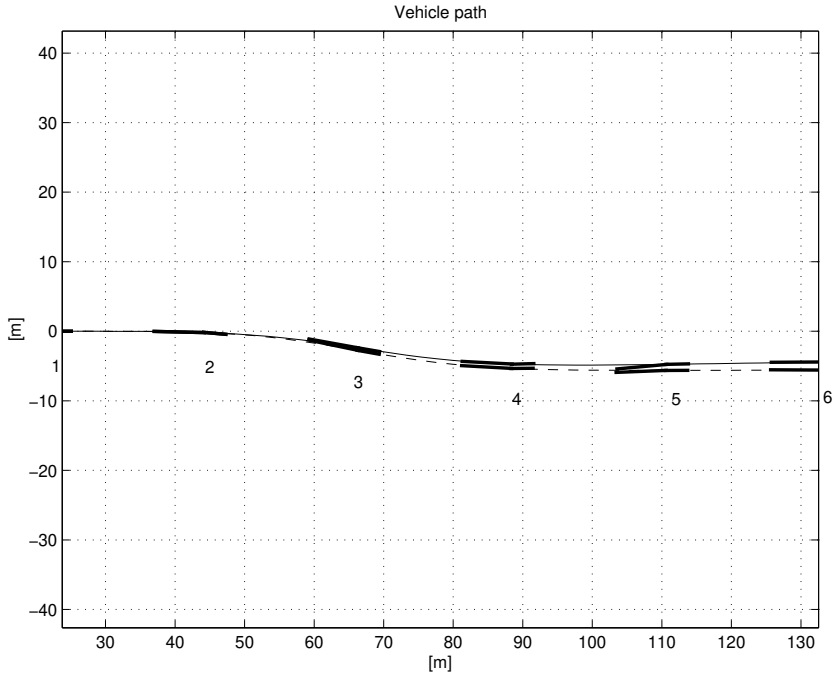

Figure 60 Vehicle trace for the linear reference model (dashed), and the controlled model with nonlinear tires.

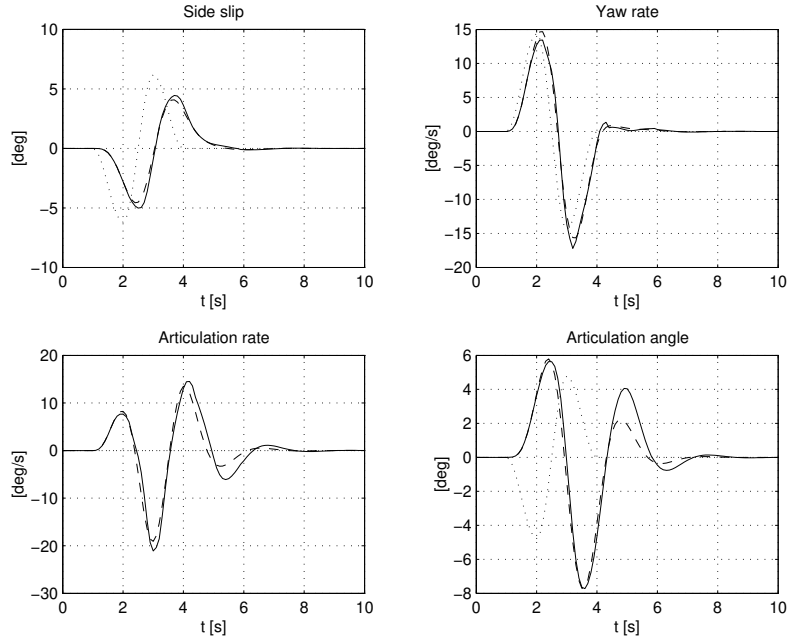

Figure 61 Vehicle states. (Solid: nonlinear model, Dashed: linear model, Dotted: steady-state)

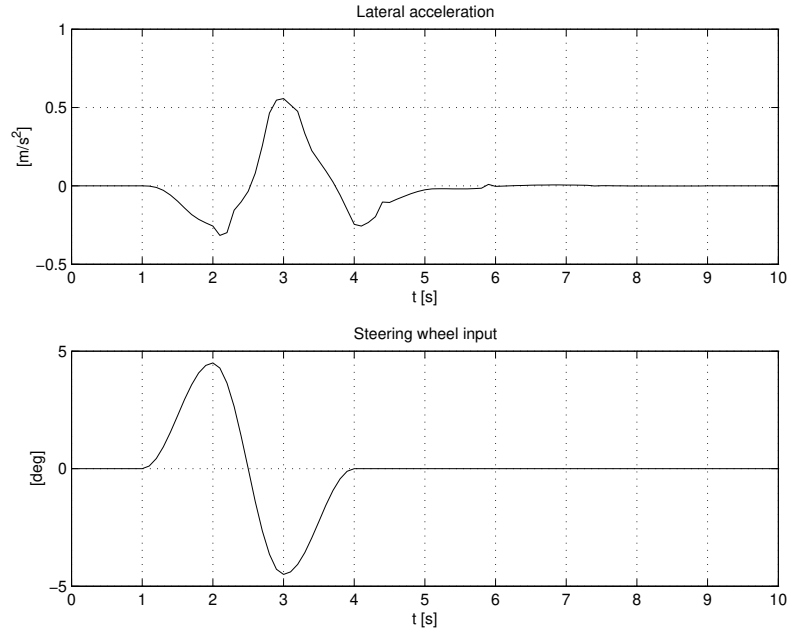

Figure 62 Lateral acceleration and steering input.

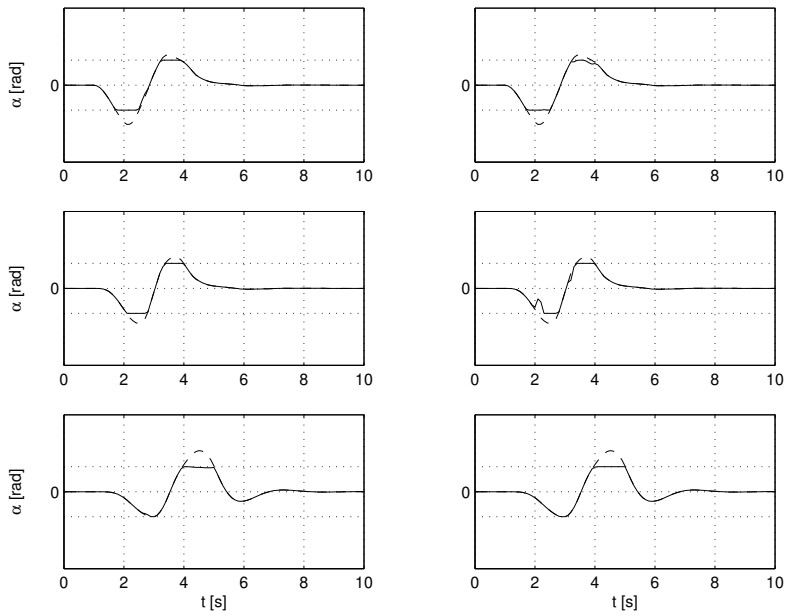

Figure 63 Side slips. (Solid: effective slip α', Dashed: actual slip α, Dotted: slip saturation limit α^*, Upper left: front left wheel, Upper right: front right wheel, Middle left: rear left wheel, Middle right: rear right wheel, Lower left: semitrailer left wheel, Lower right: semitrailer right wheel)

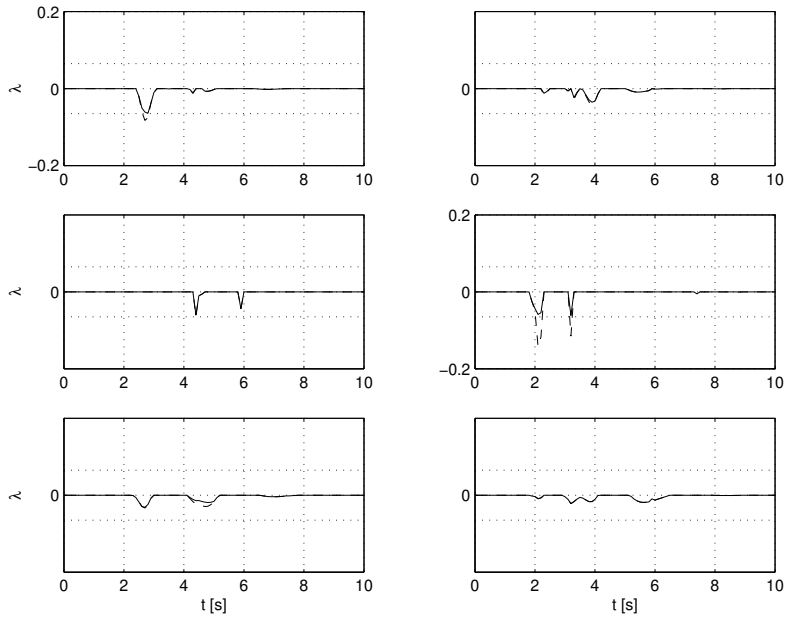

Figure 64 Longitudinal slips. (Solid: effective slip λ', Dashed: actual slip λ, Dotted: slip saturation limit λ^*, Upper left: front left wheel, Upper right: front right wheel, Middle left: rear left wheel, Middle right: rear right wheel, Lower left: semitrailer left wheel, Lower right: semitrailer right wheel)

A.11 Tractor-Semitrailer Jackknifing — Uncontrolled

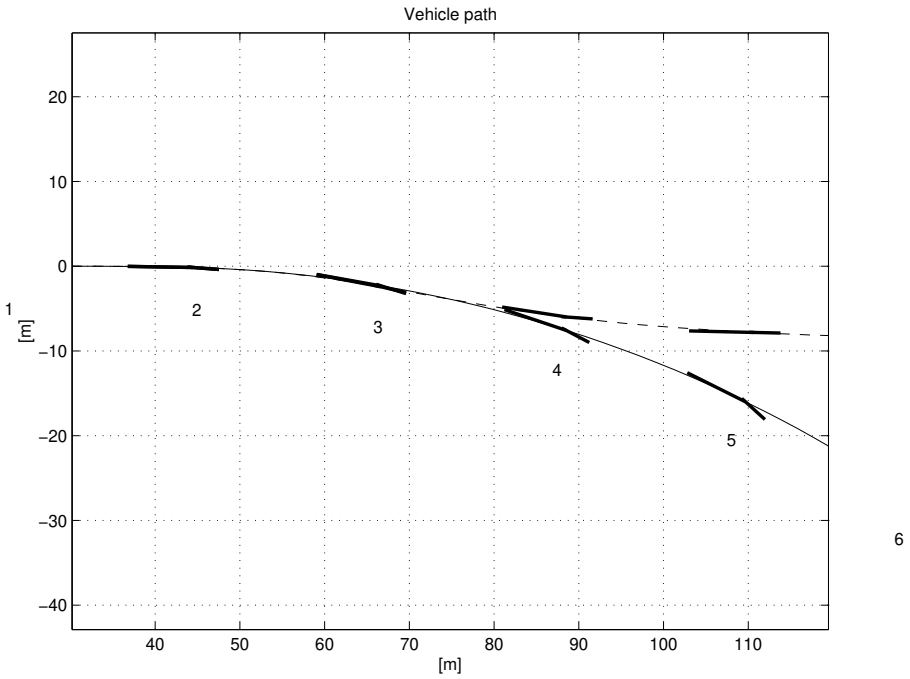

Figure 65 Vehicle trace for the linear reference model (dashed), and the controlled model with nonlinear tires.

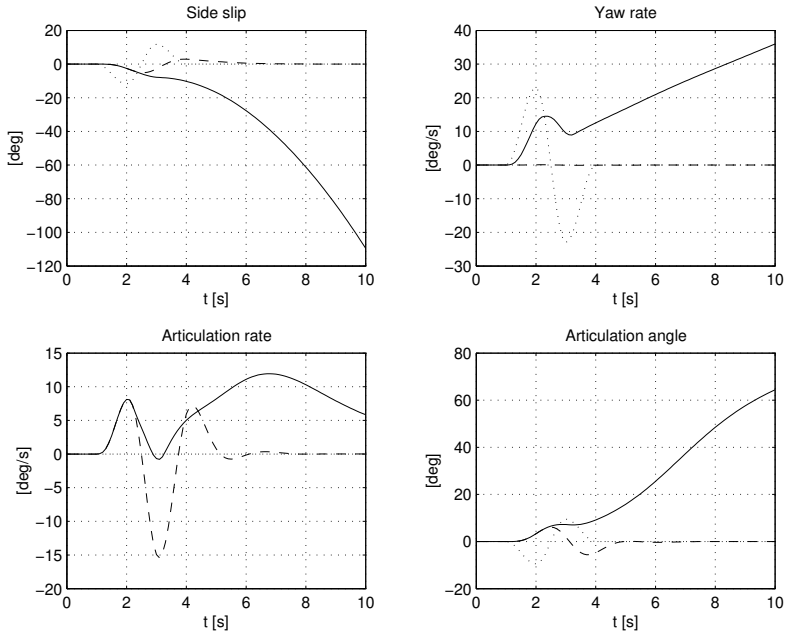

Figure 66 Vehicle states. (Solid: nonlinear model, Dashed: linear model, Dotted: steady-state)

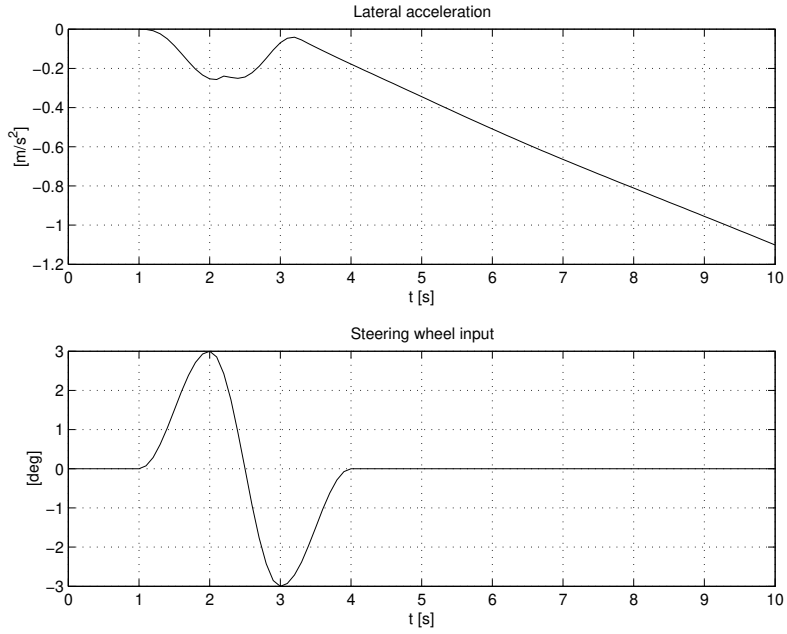

Figure 67 Lateral acceleration and steering input.

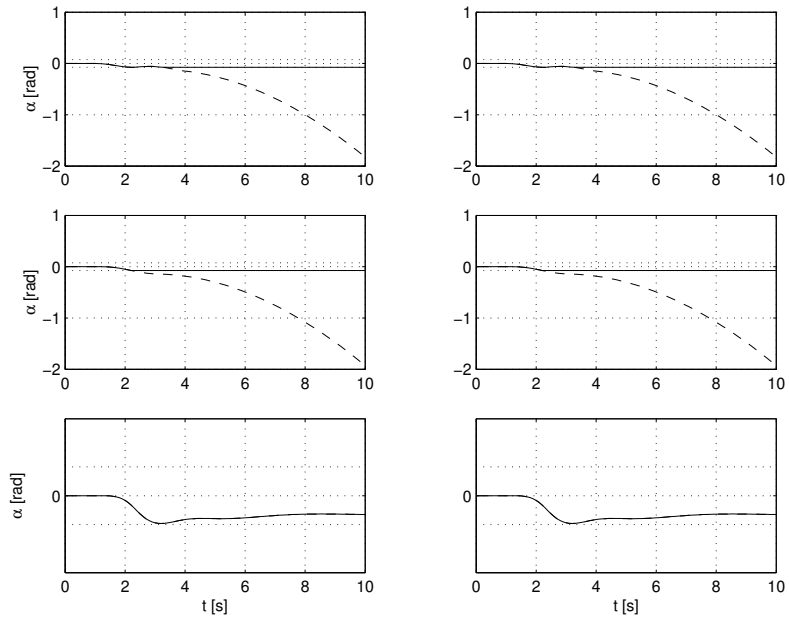

Figure 68 Side slips. (Solid: effective slip α', Dashed: actual slip α, Dotted: slip saturation limit α^*, Upper left: front left wheel, Upper right: front right wheel, Middle left: rear left wheel, Middle right: rear right wheel, Lower left: semitrailer left wheel, Lower right: semitrailer right wheel)

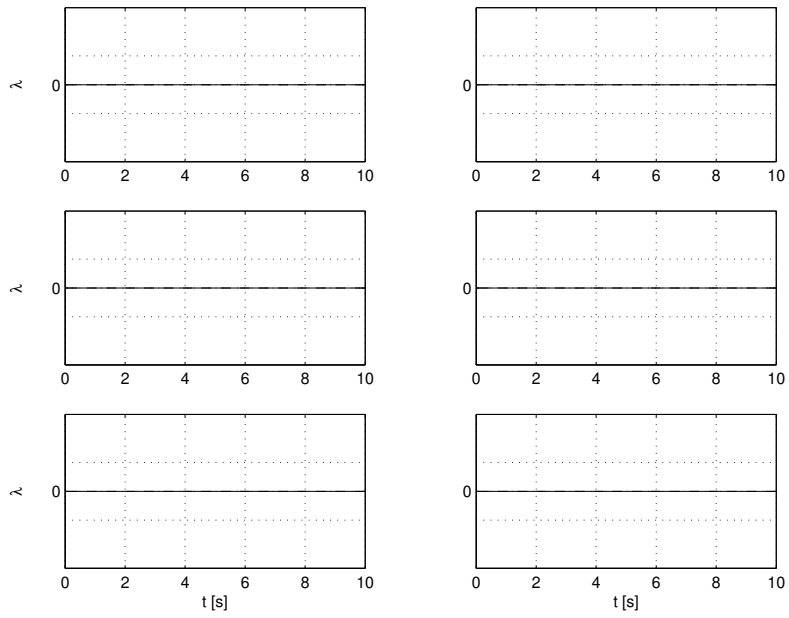

Figure 69 Longitudinal slips. (Solid: effective slip λ', Dashed: actual slip λ, Dotted: slip saturation limit λ^*, Upper left: front left wheel, Upper right: front right wheel, Middle left: rear left wheel, Middle right: rear right wheel, Lower left: semitrailer left wheel, Lower right: semitrailer right wheel)

A.12 Tractor-Semitrailer Jackknifing — Controlled Tractor

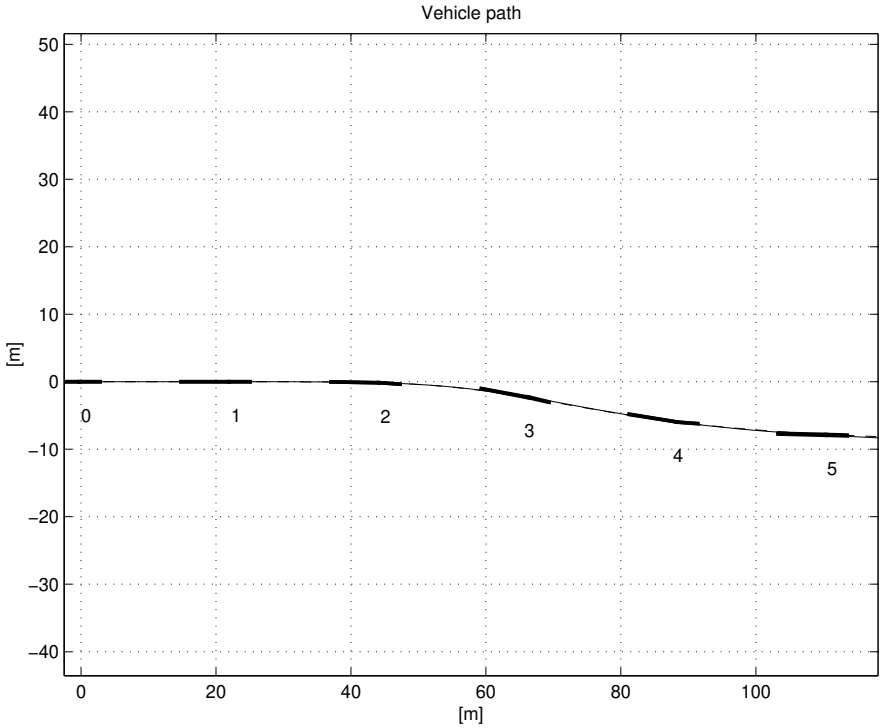

Figure 70 Vehicle trace for the linear reference model (dashed), and the controlled model with nonlinear tires.

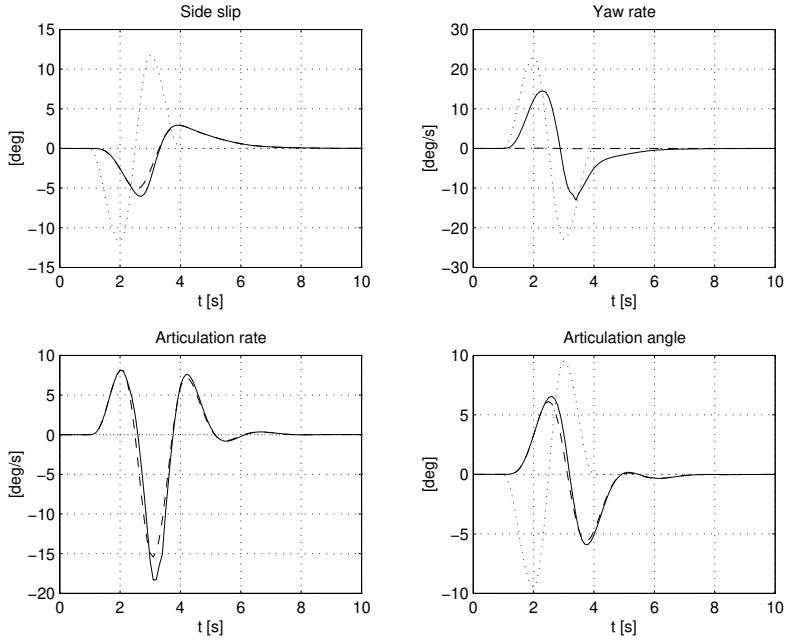

Figure 71 Vehicle states. (Solid: nonlinear model, Dashed: linear model, Dotted: steady-state)

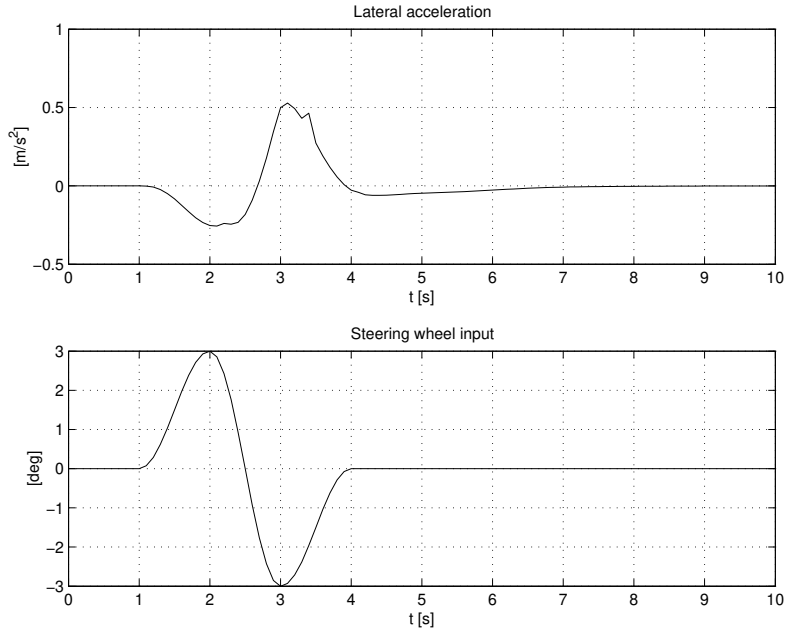

Figure 72 Lateral acceleration and steering input.

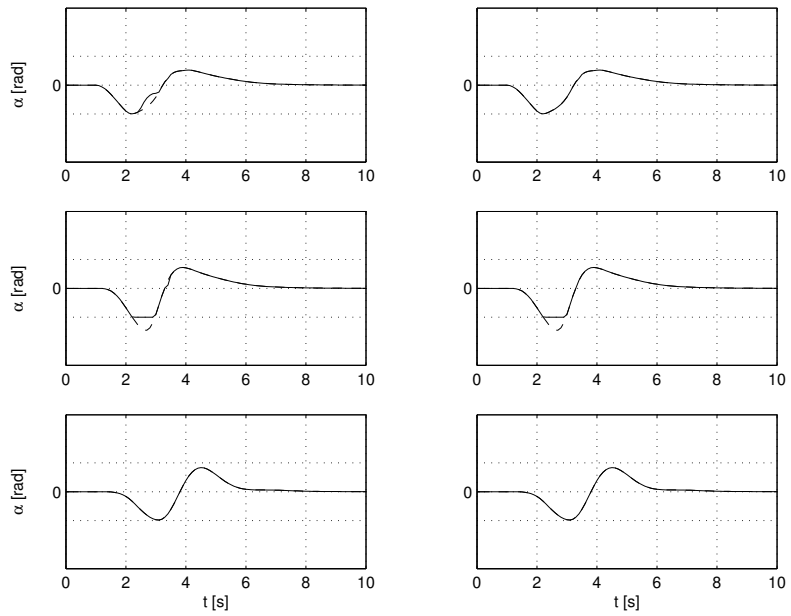

Figure 73 Side slips. (Solid: effective slip α', Dashed: actual slip α, Dotted: slip saturation limit α^*, Upper left: front left wheel, Upper right: front right wheel, Middle left: rear left wheel, Middle right: rear right wheel, Lower left: semitrailer left wheel, Lower right: semitrailer right wheel)

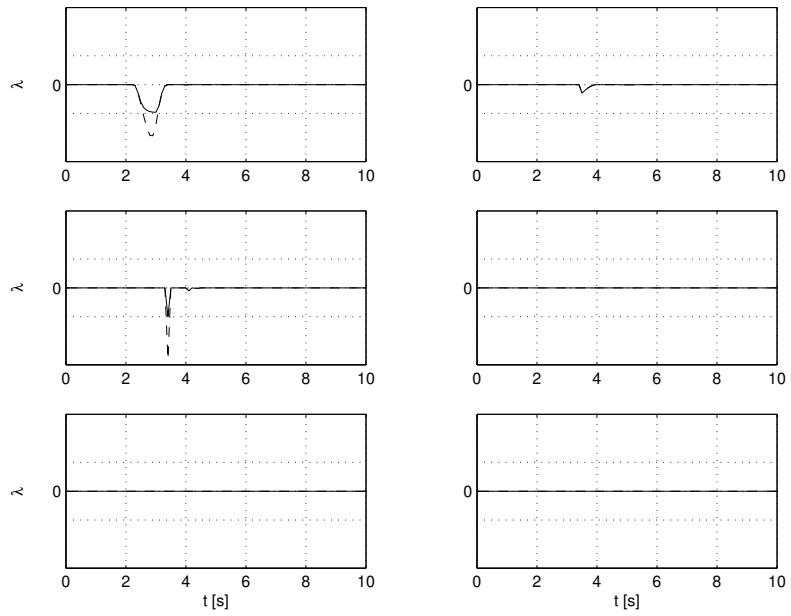

Figure 74 Longitudinal slips. (Solid: effective slip λ', Dashed: actual slip λ, Dotted: slip saturation limit λ^*, Upper left: front left wheel, Upper right: front right wheel, Middle left: rear left wheel, Middle right: rear right wheel, Lower left: semitrailer left wheel, Lower right: semitrailer right wheel)

A.13 Tractor-Semitrailer Jackknifing — Controlled Tractor and Semi-Trailer

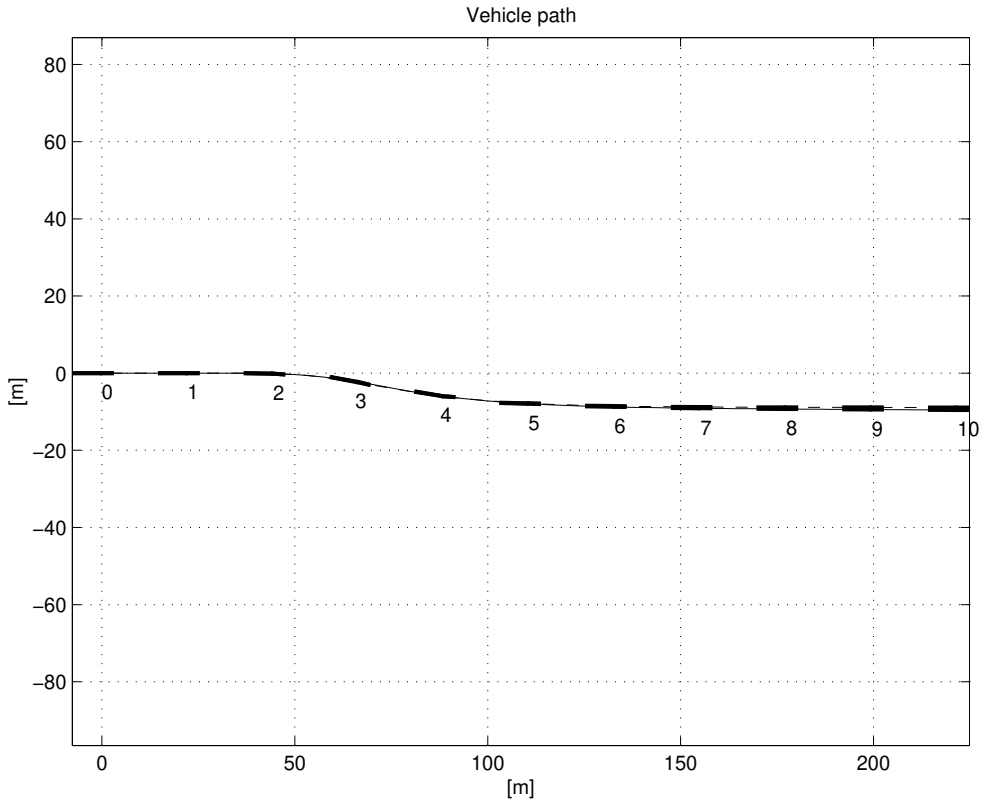

Figure 75 Vehicle trace for the linear reference model (dashed), and the controlled model with nonlinear tires.

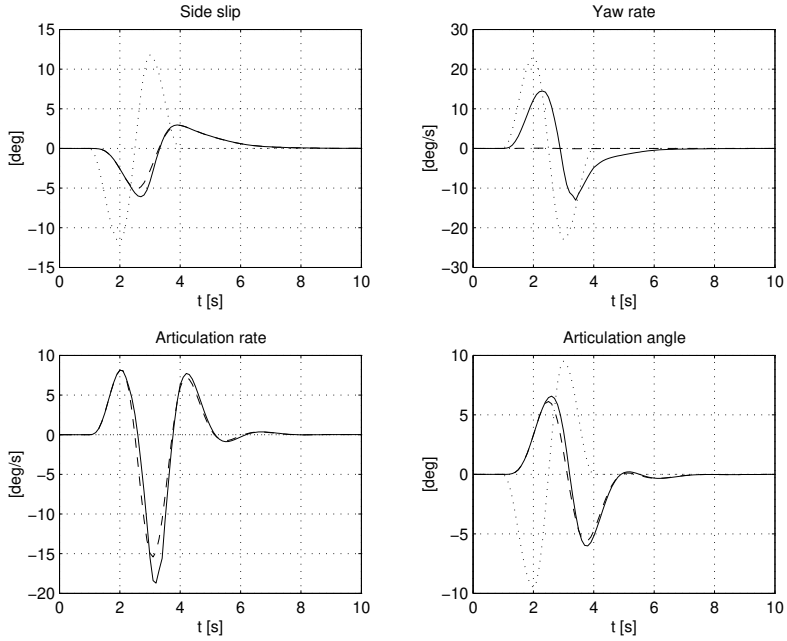

Figure 76 Vehicle states. (Solid: nonlinear model, Dashed: linear model, Dotted: steady-state)

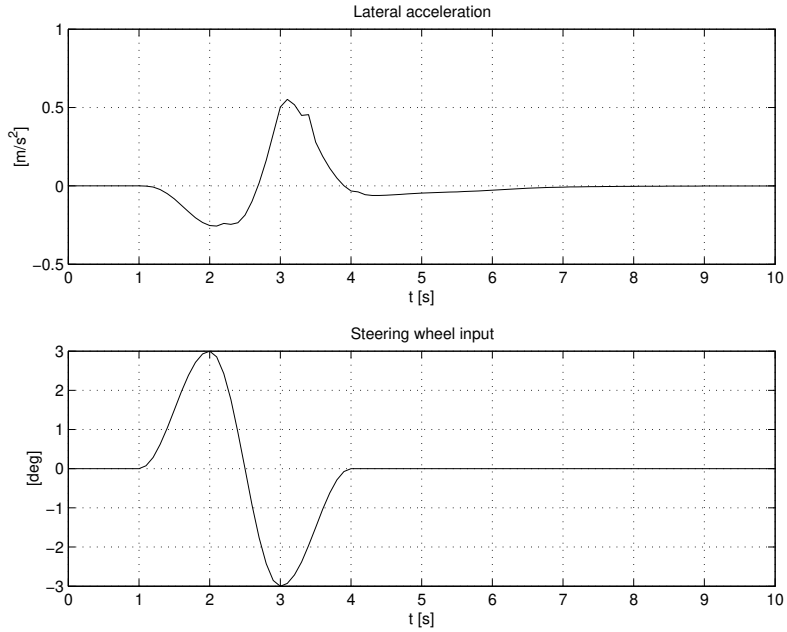

Figure 77 Lateral acceleration and steering input.

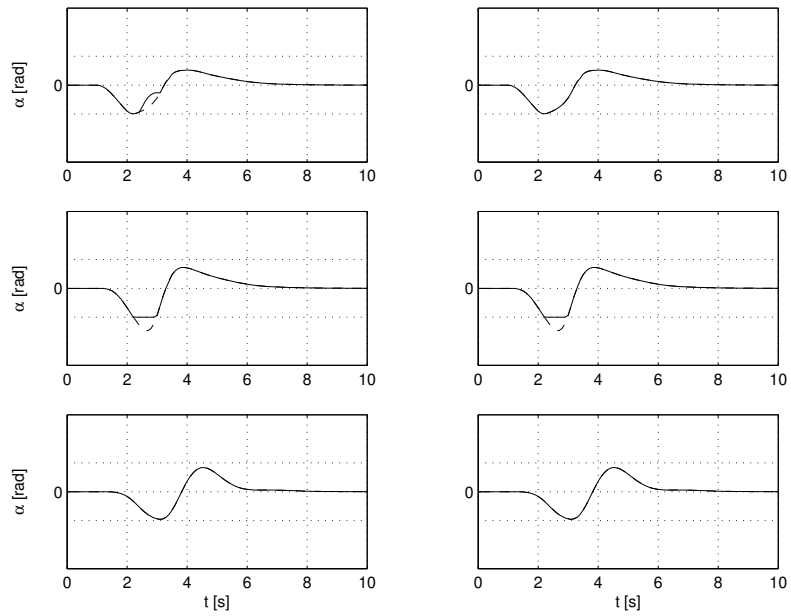

Figure 78 Side slips. (Solid: effective slip α', Dashed: actual slip α, Dotted: slip saturation limit α^*, Upper left: front left wheel, Upper right: front right wheel, Middle left: rear left wheel, Middle right: rear right wheel, Lower left: semitrailer left wheel, Lower right: semitrailer right wheel)

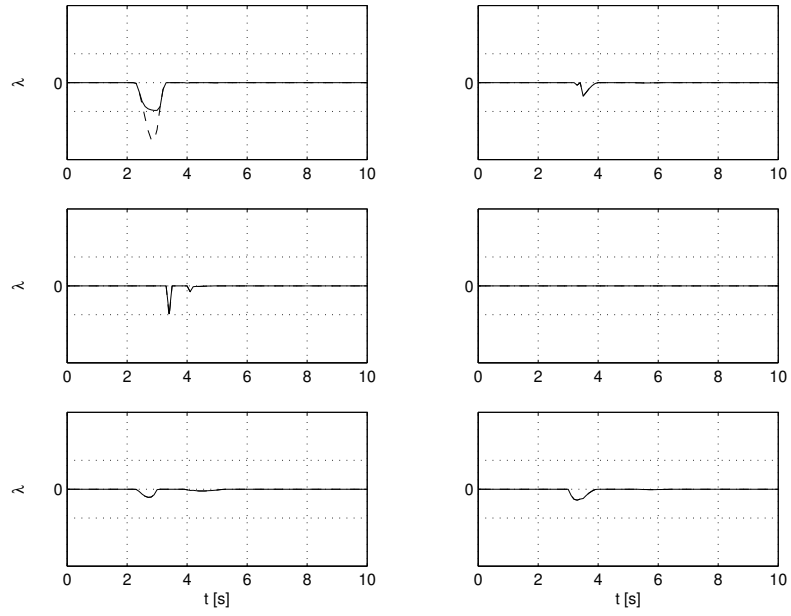

Figure 79 Longitudinal slips. (Solid: effective slip λ', Dashed: actual slip λ, Dotted: slip saturation limit λ^*, Upper left: front left wheel, Upper right: front right wheel, Middle left: rear left wheel, Middle right: rear right wheel, Lower left: semitrailer left wheel, Lower right: semitrailer right wheel)